communications biology

A Nature Portfolio journal

Article

https://doi.org/10.1038/s42003-025-07944-w

Functional maturation of preterm intestinal epithelium through CFTR activation

Jihyun Kim[1,5], Hyunji Park[1,5], Na-Young Park[1], Se In Hwang[2], Young Eun Kim[3], Se In Sung[4] ✉, Yun Sil Chang[2,3,4] ✉ & Ara Koh[1] ✉

Preterm birth disrupts intestinal epithelial maturation, impairing digestive and absorptive functions. This study integrates analysis of single-cell RNA sequencing datasets, spanning fetal to adult stages, with human preterm intestinal models derived from the ileal tissue of preterm infants. We investigate the potential of extracellular vesicles (EVs) derived from human Wharton's jelly mesenchymal stem cells to promote intestinal maturation. Distinct enterocyte differentiation trajectories are identified during the transition from immature to mature stages of human intestinal development. EV treatment, particularly with the EV39 line, significantly upregulates maturation-specific gene expression related to enterocyte function. Gene set enrichment analysis reveals an enrichment of TGFβ1 signaling pathways, and proteomic analysis identifies TGFβ1 and FGF2 as key mediators of EV39's effects. These treatments enhance cell proliferation, epithelial barrier integrity, and fatty acid uptake, primarily through CFTR-dependent mechanisms—unique to human preterm models, not observed in mouse intestinal organoids. This highlights the translational potential of EV39 and CFTR activation in promoting the functional maturation of the premature human intestine.

The human small intestine serves as a crucial interface between ingested nutrients and the body's internal environment, where its epithelium plays a pivotal role in maintaining health[1]. This role is especially vital during early life, given the rapid growth and development of infants, necessitating optimal nutrient uptake and protection from harmful microbes[2]. However, early insults to the intestinal epithelium can have profound and lasting consequences, predisposing preterm infants to a range of long-term health issues, including an increased susceptibility to gastrointestinal disorders like necrotizing enterocolitis and meconium ileus, impaired growth, neurodevelopmental disorders, and chronic diseases[3–5].

Preterm birth, occurring before 37 completed weeks of gestation and typically after 27 weeks for live births, presents a significant challenge to the proper development and function of the intestinal epithelium[6–9]. This challenge arises from the disruption of fetal intestinal development during the third trimester of pregnancy when functional intestinal maturation peaks[8,10,11]. Consequently, preterm infants are left with immature gastrointestinal systems ill-equipped to handle the demands of enteral nutrition[12,13]. Thus, enhancing intestinal epithelial maturation stands out as a critical avenue for improving the functionality of preterm infants and addressing the subsequent long-term health issues they are likely to encounter.

While our understanding of intestinal maturation comes largely from mouse studies, differences between mouse and human intestinal development exist. Mouse studies suggest that intestinal morphogenesis concludes several weeks after birth, contrasting with humans, where it is completed prior to birth[14,15]. Recent advancements in single-cell RNA sequencing (scRNA-seq) have shed light on key disparities in gut epithelium lineage marker genes between mice and humans, particularly in cell types like intestinal stem cells, Paneth cells, and goblet cells[16]. For example, mouse Paneth cells are enriched in factors supporting intestinal stem cells, while human Paneth cells express antimicrobial genes[17–20]. Moreover, scRNA-seq has identified a unique subtype of mature absorptive cells, BEST4+ cells, present only in the human intestinal epithelium[21]. However, their absence in mouse intestines poses challenges for functional studies aimed at understanding their roles.

[1]Department of Life Sciences, Pohang University of Science and Technology (POSTECH), Pohang, 37673, South Korea. [2]Department of Health Sciences and Technology, Samsung Advanced Institute for Health Sciences & Technology (SAIHST), Sungkyunkwan University, Seoul, 06351, South Korea. [3]Cell and Gene Therapy Institute, Samsung Medical Center, Seoul, 06351, South Korea. [4]Department of Pediatrics, Samsung Medical Center, Sungkyunkwan University School of Medicine, Seoul, 06351, South Korea. [5]These authors contributed equally: Jihyun Kim, Hyunji Park. ✉e-mail: sein.sung@samsung.com; cys.chang@samsung.com; ara.koh@postech.ac.kr

Mesenchymal stem cells (MSCs), sourced from tissues like bone marrow and Wharton's jelly of human umbilical cord, are renowned for their regenerative potential, capable of self-renewal and differentiation into various cell lineages[22,23]. Recent research highlights that the therapeutic efficacy of MSCs primarily relies on their paracrine secretion, notably through the release of extracellular vesicles (EVs)[24]. These EVs carry bioactive molecules derived from parent cells, including growth factors, chemokines, cytokines, mRNAs, and miRNAs, which can be delivered to target cells[24]. Utilizing MSC-derived EVs presents considerable advantages over live cells, providing a higher safety profile, reduced immunogenicity, and mitigated risk of tumor formation[25]. Thus, MSC-derived EVs represent an innovative cell-free therapy with compelling advantages over parent MSCs, holding significant potential for driving tissue repair and regeneration[26]. However, research on the role of MSC-derived EVs in intestinal epithelium maturation remains limited.

In this study, we thus aim to investigate the effects of EVs derived from human Wharton's jelly- derived MSC on human intestinal organoids derived from preterm infants, leveraging the presence of BEST4+ cells in human intestinal organoids[27,28]. Our objective is to identify which small intestinal cell types undergo significant maturation from the fetal stage to pediatric and adult stages using scRNA-seq data sourced from a published database comprising 96 samples[16,29–34]. Additionally, we seek to determine which specific components of MSC-derived EVs can facilitate intestinal maturation through proteomic analysis of EVs.

Results

Developmental dynamics of the human small intestine from fetal to adult stages

To explore the continuum of developmental dynamics of human small intestine, we incorporated recently published scRNA-seq data from a total of seven studies, specifically focusing on small intestinal samples[16,29–34]. This dataset comprises 96 samples spanning a wide age range from 8 to 24 gestational age (GA) to 70 years old (Fig. 1a, Supplementary Table 1). To ensure data consistency across studies, we corrected for batch effects using harmony[35] after filtering out low-quality cells. This resulted in a substantially integrated embedding in which cells grouped by cell type across various studies (Supplementary Fig. 1a). Shared nearest neighbor (SNN) modularity optimization-based clustering and marker gene-based annotation yielded a total of 298,224 high-quality cells representing epithelial, mesenchymal, immune, endothelial, neuronal, and erythroid cells (Supplementary Fig. 1b, c)[36].

To refine our analysis and specifically focus on epithelial cells within the small intestine, we isolated small intestinal epithelial cell populations (*EPCAM* +, *CDH1* +, *KRT8* +, *KRT18* +, *FXYD3* +, *PERP* +), comprising 82,144 cells. Our integrated uniform manifold approximation and projection (UMAP) encompassing fetal to pediatric/adult small intestinal epithelium scRNA-seq data identified differentially positioned epithelial cells depending on sample age (1st trimester, 2nd trimester, and pediatric/adult), inferring age-dependent epithelial characteristics (Fig. 1b). Subsequently, we manually annotated each cluster based on specific epithelial cell type markers (Supplementary Fig. 1d). This comprehensive cluster annotation enabled the identification of 10 distinct cell types within both fetal and adult small intestines (Fig. 1c). These cell types include intestinal stem cells (ISCs), progenitor cells, transit-amplifying cells (TAs), Paneth cells, enterocyte precursors, enterocytes, BEST4+ enterocytes, goblet cells, enteroendocrine cells (EECs), and tuft cells. The proportion of these cell types at each developmental stage showed age-dependent alterations, including elevated populations of enterocytes, BEST4+ enterocytes, Paneth cells, goblet cells, and tuft cells and a decrease in progenitors, TAs, and EECs in pediatric/adult compared to fetal stages (Fig. 1d, Supplementary Fig. 1e), aligning with previously reported maturation trends[16].

Next, we performed RNA velocity analysis along with partition-based graph abstraction (PAGA) on individual fetal and pediatric/adult epithelial cells. These approaches provided velocity-inferred directionality and topological similarity, allowing us to infer lineage trajectories to understand cell differentiation dynamics and analyze transcriptomic similarities between cell types in different clusters[37,38]. This enabled us to estimate the connectivity between cell types during fetal and pediatric/adult epithelial development, respectively (Fig. 1e, f, Supplementary Fig. 1f, g). Our analysis revealed unique differentiation trajectories from ISCs to enterocytes between fetal and pediatric/adult stages (Fig. 1e, f). In the fetal stages, the trajectories and PAGA connectivity graph showed predominant involvement of proximal progenitors in early enterocyte development, a feature identified in various scRNA-seq studies[16,30,39]. Additionally, we observed that BEST4+ enterocytes were exclusively connected to ISCs within adult epithelial cells, while in fetal epithelial cells, a significant transcriptomic distance with no connectivity between cell types was identified (Supplementary Fig. 1f, g). This supports the notion that BEST4+ enterocytes represent a novel subtype of mature absorptive cells[16] and may participate in epithelial maturation of the human intestine. Collectively, the differences in cell type abundance and the interconnected dynamics of epithelial cells between fetal and pediatric/adult stages clearly demonstrate that the human small intestinal epithelium significantly differs between these developmental stages.

Delineating divergent differentiation trajectories of enterocytes across fetal and pediatric/adult intestinal development

To investigate epithelial transition across intestinal development, we constructed developmental trajectory map using monocle 3[40], where cells were ordered and positioned along a pseudotime trajectory representing the biological process of cell differentiation and development (Fig. 2a). The pseudotime trajectory indicated a common path originating from ISCs and oriented toward secretory (EEC, goblet) differentiation trajectories in both fetal and pediatric/adult stages (Fig. 2a). However, there was markedly distinct path from ISCs to enterocyte between fetal and pediatric/adult stages (Fig. 2a).

We thus isolated both fetal and adult enterocyte developmental branches, from ISC, proximal progenitor, enterocyte precursor and enterocyte. Then, we identified 155 fetus-specific and 28 adult-specific enterocyte lineage genes that changed along the established virtual time scale, based on multi-directional and multi-dimensional spatial autocorrelation (Moran's I test) (Supplementary Table 2). The fetal enterocyte lineage was predominantly associated with regulation of protein stability (*PLPP3, EFNA1, GLMP, ATP1B3, NPM1, PIM1, HSP90AB1, APOA1*) and positive regulation of proteolysis (*S100A10, EFNA1, MELTF, DAB2, RACK1, CLDN4, MYC, HMGB1*) as indicated by Gene Ontology (GO) annotations (Supplementary Fig. 2a). On the other hand, the adult enterocyte lineage was associated with lipid transport (*CIDEC, FABP2, ACSL5, PRAP1, APOA4, ACE*) and fatty acid metabolic process (*FABP2, CYP3A4, ACSL5, APOA4, CES2*) (Supplementary Fig. 2b). Our findings indicate that enterocytes in fetal and pediatric/adult stages follow stage-specific differentiation trajectories, molecular characteristics, and potentially functional features.

We thus investigated differences in functional potential between fetal and pediatric/adult enterocytes. First, we classified each cell type cluster, designating clusters in the fetal samples as 'I' and in the pediatric/adult samples as 'II' (Supplementary Fig. 2c). By extracting a subset of the data, including 30,720 absorptive enterocytes, we observed clear separation between enterocyte type I and type II (Fig. 2b). Differential expression analysis between type I and type II enterocytes identified 883 type II enterocyte-enriched genes. When plotted based on sample age, these genes further verified their enrichment in pediatric/adult stages compared to the 1st and 2nd trimesters (Supplementary Fig. 2d). By plotting type II enterocyte-enriched genes in the UMAP we generated, we further narrowed down and identified genes specific to adult enterocytes (Fig. 2c), as well as those showing higher expression in the adult than in the fetal enterocytes (Fig. 2d). In contrast, well-known enterocyte marker genes such as *FABP2, APOA4, RBP2*, and *ANPEP* showed expression across various intestinal cell types, with the exception for *APOA4* (Supplementary Fig. 2e). While *FABP2, APOA4*, and *ANPEP* were slightly more enriched in adult than in fetal

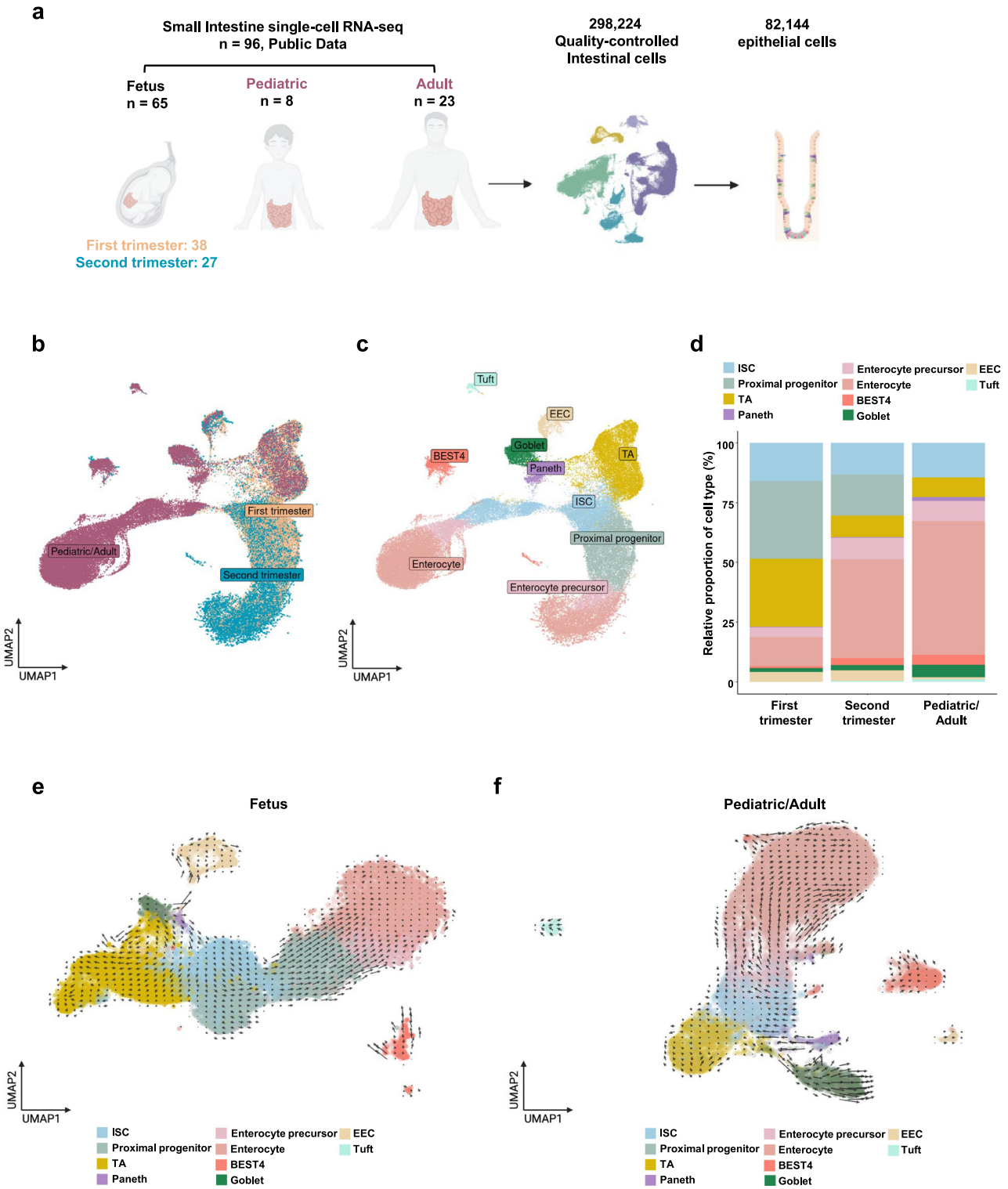

Fig. 1 | Distinct differentiation trajectories in the small intestinal epithelium between fetal and pediatric/adult stages. a Schematic illustration showing the public data information used in our study and workflow of single-cell RNA sequencing (scRNA-seq) analysis. A total of 298,224 quality-controlled intestinal cells were generated from publicly available 96 small intestinal scRNA-seq datasets, and subsequently, 82,144 epithelial cells were isolated for downstream analysis. First trimester, 8 < gestational age (GA) < 14; Second trimester, 14 ≤ gestational age (GA) < 24; Pediatric, 4 ≤ years ≤ 12; Adult, 25 ≤ years < 70. Uniform manifold approximation and projection (UMAP) of epithelial scRNA-seq data colored by sample age (first trimester, second trimester, and pediatric/adult) (**b**) and epithelial cell type (**c**) from public scRNA-seq data of the small intestinal epithelium. BEST4, BEST4+ enterocyte; ISC, intestinal stem cell; EEC, enteroendocrine cell; TA, transit-amplifying. **d** Relative proportions of epithelial cell types at each sample age (first trimester, second trimester, and pediatric/adult). UMAP of fetal (first trimester and second trimester) (**e**) and pediatric/adult (**f**) epithelial cells with arrows indicating inferred scVelo differentiation trajectories. See also Supplementary Fig. 1.

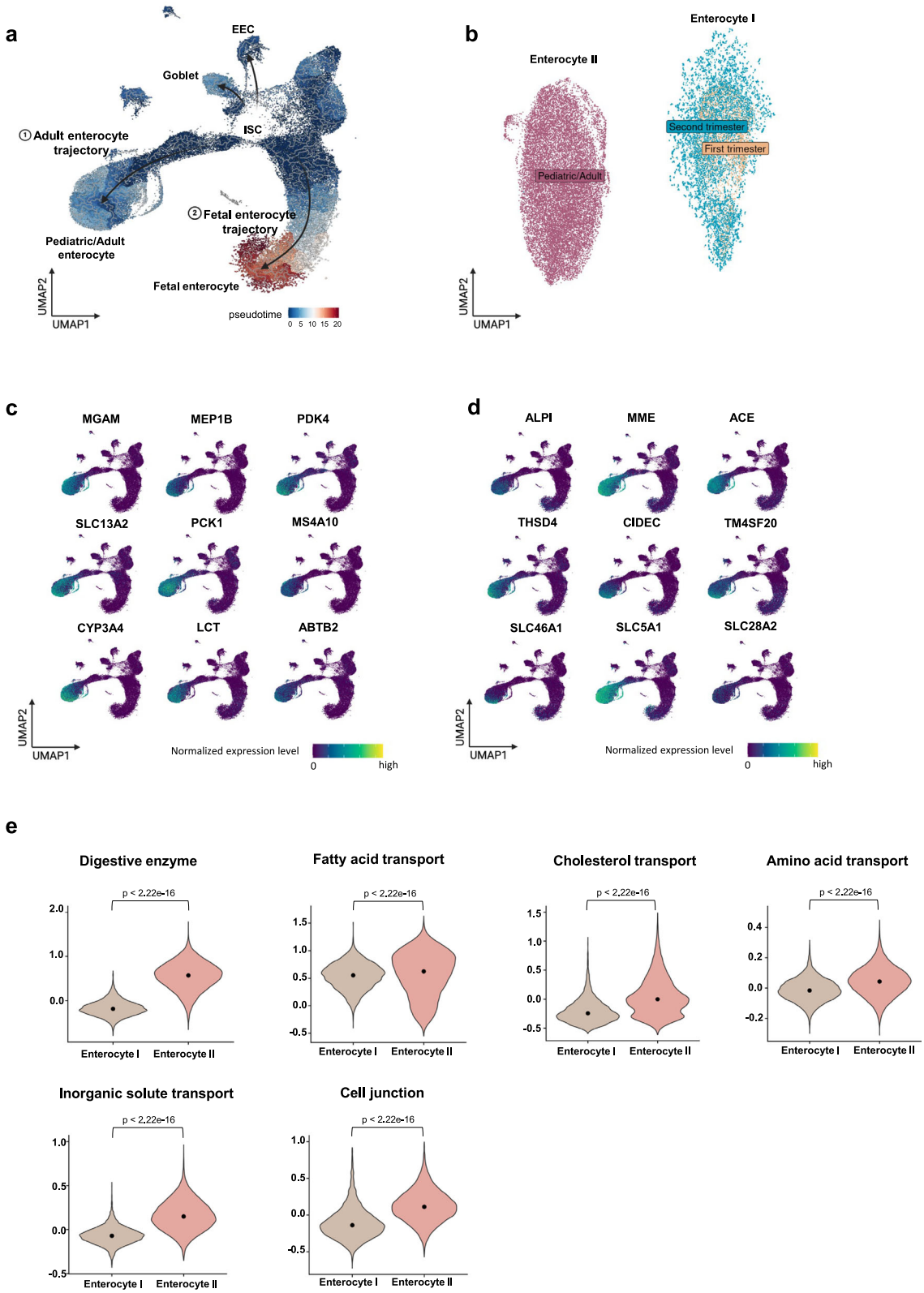

Fig. 2 | Distinct differentiation trajectories and functional potential of enterocytes in fetal versus pediatric/adult stages. a Developmental trajectories of fetal and pediatric/adult epithelial cells visualized on a uniform manifold approximation and projection (UMAP) plot, colored by pseudotime. Arrows depict differentiation paths of absorptive (fetal enterocyte and pediatric/adult enterocyte) and secretory (Goblet and enteroendocrine cell; EEC) lineages, originating from intestinal stem cells (ISCs). **b** UMAP of enterocyte type I (fetal-like, first trimester and second trimester) and enterocyte type II (adult-like, pediatric/adult) colored by sample age (first trimester, second trimester and pediatric/adult). Feature plots showing the expression of adult enterocyte marker genes that were specific to enterocyte type II (**c**) and abundant in enterocyte type II (**d**). **e** Violin plots showing the mean expression of enterocyte functionalities (digestive enzyme, fatty acid transport, cholesterol transport, amino acid transport, inorganic solute transport, cell junction) in enterocyte type I and II. Significant functional enhancement was observed in enterocyte type II across all categories ($p < 2.22e{-}16$, Wilcoxon rank-sum test). See also Supplementary Fig. 2.

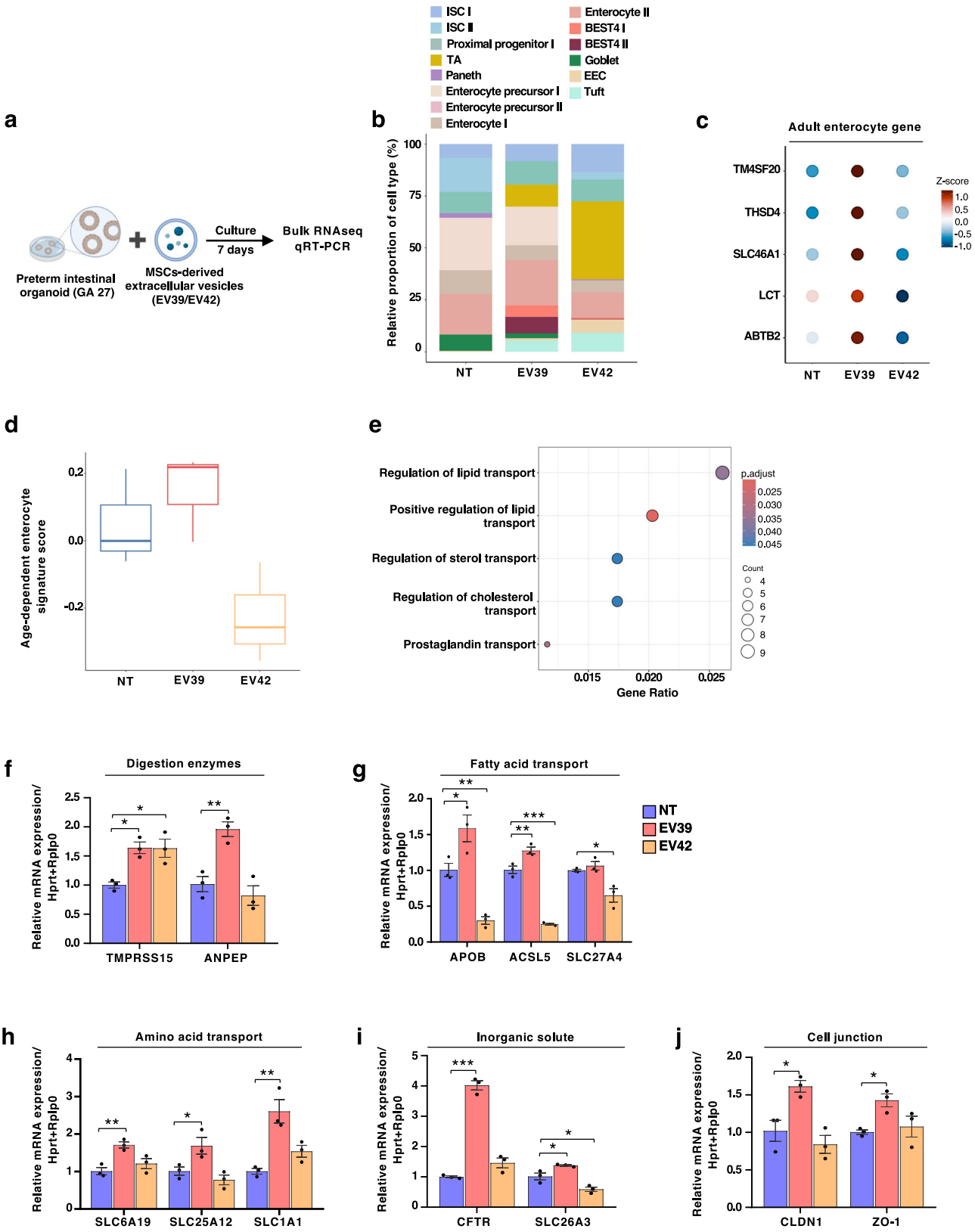

enterocytes (Supplementary Fig. 2e), our analysis suggests the presence of mature enterocyte-specific markers.

Among these adult enterocyte markers (Fig. 2c, d), *LCT, MGAM, MEP1B, CYP3A4, SLC5A1, SLC28A2, ALPI*, and *PCK1* have been previously reported as mature enterocyte-expressing genes[31,41–47]. Our analysis also identified novel mature enterocyte markers such as *MME, ACE, CIDEC, SLC46A1, SLC13A2, PDK4, MS4A10, ABTB2, THSD4*, and *TM4SF20*. These markers were previously known to be expressed in the intestine but not specifically in mature enterocytes. *MME* (membrane metalloendopeptidase), also known as neprilysin, inactivates several

Fig. 3 | Effects of mesenchymal stem cell (MSC)-derived extracellular vesicles (EVs) on enterocyte maturation in human preterm intestinal epithelial cells. **a** Schematic illustration of the experimental procedure showing treatment of preterm intestinal epithelial cells with mesenchymal stem cell (MSC)-derived extracellular vesicles (EVs, EV39 and EV42, 2×10^9 EVs/mL for seven days), followed by bulk RNA-seq and qRT-PCR analysis. **b** Relative proportions of epithelial cell types estimated by deconvolution of bulk RNA-seq data from preterm intestinal epithelial cells treated with MSC-derived EVs (EV39 and EV42, 2×10^9 EVs/mL for seven days), based on previously analyzed scRNA-seq profiles of small intestinal epithelial cells. NT, non-treated group, BEST4, BEST4+ enterocyte; ISC, intestinal stem cell; EEC, enteroendocrine cell; TA, transit-amplifying. **c** Dot plot showing Z-score transformed relative expression of adult enterocyte marker genes (*TMSF20, THSD4, SLC46A1, LCT, ABTB2*) in the human preterm intestinal epithelial cells treated with MSC-derived EVs (EV39 and EV42, 2×10^9 EVs/mL) for seven days. NT, non-treated group. **d** Box plot showing the abundance of age-dependent enterocyte gene sets (first trimester < second trimester < pediatric/adult, n = 224, Supplementary Table 2). NT, non-treated group. Box plot presents minimum, 25% quartile, median, 75% quartile, maximum. **e** Dot plot showing gene ontology terms obtained from significantly upregulated genes in the preterm intestinal epithelial cells treated with MSC-derived EVs (EV39, 2×10^9 EVs/mL) for seven days compared to non-treated group. Relative mRNA expression of functional enterocyte markers: digestive enzyme genes (**f**), fatty acid transporter genes (**g**), amino acid transporter genes (**h**), inorganic solute transporter genes (**i**), and cell junction genes (**j**) in the preterm intestinal epithelial cells treated with MSC-derived EVs (EV39 and EV42, 2×10^9 EVs/mL) for seven days. mRNA level of each gene is normalized to *HPRT1* and *RPLP0* level. NT, non-treated group ($n = 3$, 3 wells per group, NT vs. other groups). Quantitative data are expressed as the mean ± standard error of the mean (S.E.M). $^*P < 0.05$, $^{**}P < 0.01$, $^{***}P < 0.001$. *P* values were determined by one-way ANOVA with Dunnett's post hoc test (**f**–**j**). See also Supplementary Fig. 3.

peptides[48–50] and might have the potential to regulate gut-derived peptide hormones based on its expression in the differentiated small intestinal epithelium[51,52]. *ACE* (Angiotensin I converting enzyme), which converts angiotensin I to angiotensin II, is involved in blood pressure regulation[53] and has shown roles in intestinal homeostasis, including terminal digestion of peptides[49], cell turnover[54] and glucose uptake inhibition via local production of angiotensin II[55]. *PDK4* (pyruvate dehydrogenase kinase 4) is known to switch glucose catabolism to fatty acid utilization[45]. Similarly, *CIDEC* (cell death-inducing DNA fragmentation-factor like effector C), known as fat-specific protein Fsp27, plays a role in intestinal lipid absorption[56], aligning with the enrichment of fatty acid metabolic process in adult enterocytes (Supplementary Fig. 2f). *SLC13A2* (sodium-dicarboxylate cotransporter) absorbs citric acid cycle intermediates such as succinate, a-ketoglutarate, and citrate, with high selectivity for succinate[57]. *SLC46A1* (proton-coupled folate transporter) mediates obligatory intestinal folate absorption[58,59]. Both succinate and folate are produced by gut microbes, with succinate crossing epithelial cells via *SLC13A2* to regulate immune cells[57], reflecting the microbial environment differences between fetal and adult intestines. *MS4A10*, a member of the recently identified MS4A/CD20 protein family, is exclusively expressed in the intestine[60]; however, its specific role within the intestinal environment remains unclear. *ABTB2* (ankyrin repeat and BTB domain-containing 2), *THSD4* (thrombospondin type 1 domain-containing 4), and *TM4SF20* (transmembrane 4 L six family member 20) have been detected through intestinal tissue staining and RNA sequencing data from the 2024 Human Protein Atlas[61], but their precise contributions in the small intestine are yet to be elucidated.

Furthermore, gene set enrichment analysis (GSEA) with type I and type II enterocyte genes showed an enrichment of duodenal mature enterocyte gene sets[62] in type II enterocytes and an enrichment of immature organ gene sets (i.e., fetal thymus stromal cells and fetal spleen AFP ALB positive cells)[63] in type I enterocytes (Supplementary Fig. 2g), supporting the functional maturity differences between the two types of enterocytes. In the context of metabolism, type II enterocytes were specialized for lipid metabolic processes, small molecule metabolic processes, and eicosanoid metabolic processes. In contrast, type I enterocytes were specialized for chondroitin sulfate/dermatan sulfate metabolism, sialic acid metabolism, fat-soluble vitamin metabolism, and amino acid metabolic processes (Supplementary Fig. 2f). To quantitatively compare the metabolic and functional capacity of type I and II enterocytes, metabolic module scores were calculated by averaging the expression of functional genes involved in fatty acid transport and processing, digestive enzymes, cholesterol transporters, amino acid transporters, cell junctions, inorganic solute transporters, and organic transporters, respectively (Supplementary Fig. 2h–m). As expected, metabolic module scores across each enterocyte function were significantly higher in type II enterocytes than in type I enterocytes (Fig. 2e), supporting the advanced metabolic functionality of adult-type (type II) enterocytes[29].

Mesenchymal stem cell-derived extracellular vesicles-induced enrichment of adult-type enterocyte signatures in human preterm intestinal epithelial models

To explore the potential impact of MSCs-derived extracellular vesicles (EVs) on preterm intestinal epithelial maturation, we prepared MSCs-derived EVs and established human preterm intestinal epithelial models. MSCs were obtained from the Wharton's jelly of two distinct donors (lot39 and lot42) and validated for the expression of surface markers CD90, CD73, and CD105, while lacking CD14, CD45, and HLA-DR (Supplementary Fig. 3a, b). These MSCs were preconditioned with thrombin to enhance the EV production[64,65] and therapeutic efficacy[66]. The isolated thrombin-preconditioned MSC-derived EVs (designated as EV39 and EV42), which exhibited similar sizes and concentrations (Supplementary Fig. 3c), were characterized by the presence of EV-positive markers TSG101 and FLOT-1 and the absence of EV-negative marker GM130 (Supplementary Fig. 3d). Human preterm intestinal epithelial models were developed from organoids derived from ileal tissue obtained one week after birth from a male preterm neonate born at a gestational age (GA) of 27 weeks, who was not diagnosed with necrotizing enterocolitis. The preterm intestinal organoids were subsequently treated with EV39 and EV42 for seven days and subjected to transcriptomic profiling via RNA-seq (Fig. 3a).

First, we transformed the epithelial scRNA-seq data into bulk-like data using pseudobulk methods. This approach aggregates count values from each sample and cell type to create data that can be analyzed using the same methods as bulk RNA-seq data, which has been shown to be superior for differential gene analysis compared to single-cell methods[67]. To assess the maturity extent of the preterm intestinal organoids we established, we then plotted these pseudobulk data onto the principal component analysis (PCA) plane alongside bulk-transcriptomics data from preterm intestinal organoids. The PCA analysis indicated that the maturity of preterm intestinal organoids aligns between the second trimester and pediatric/adult stages, with closer proximity to the second trimester (Supplementary Fig. 3e). To address potential donor variability, an additional preterm intestinal organoid line, GA24, was established from ileal tissue obtained one week after birth from a female neonate born at GA24. Transcriptomic profiling of GA24 organoids revealed clustering similar to the preterm intestinal organoids (GA27) on the PCA plane, confirming their alignment between the second trimester and pediatric/adult stages (Supplementary Fig. 3e). This finding validates our models as retaining prematurity and thus suitable for analyzing the effects of EVs on human premature intestinal maturation.

We subsequently inferred cell-type composition by deconvoluting bulk RNA-seq data from EV39 or EV42-treated preterm intestinal organoids to investigate whether EV39 or EV42 could increase the population of mature cell types identified in pediatric/adult stages. Intriguingly, the estimated proportions of metabolically and functionally mature type II enterocytes were enriched by EV39 but not by EV42 (Fig. 3b). Additionally, BEST4+ enterocytes, a recently identified novel subtype of absorptive cells predominantly enriched in mature enterocytes[16] and unique to the human intestinal epithelium[21], showed increased estimated proportions in EV39-

treated premature intestinal organoids (Fig. 3b). This suggests that our premature intestinal epithelial model is functional and capable of detecting maturation signals that induce BEST4+ cells. Importantly, among the genes we identified as highly enriched in adult enterocytes (Fig. 2c, d), *TM4SF20*, *THSD4*, *SLC46A1*, *LCT*, and *ABTB2* were upregulated in EV39-treated but not in EV42-treated premature intestinal organoids (Fig. 3c, Supplementary Fig. 3f), aligning with elevated estimated proportions of mature type II enterocytes. Notably, EV39 consistently induced the expression of mature type II enterocyte-enriched genes, including *TM4SF20*, *SLC46A1*, *LCT*, and *ABTB2* in GA24 organoids (Supplementary Fig. 3g), corroborating the efficacy of EV39 across human preterm intestinal epithelial models.

Mesenchymal stem cell-derived extracellular vesicles-induced enrichment in functional genes for digestive capacity and nutrient absorption in human preterm intestinal epithelial models

Given the increased proportion of mature type II enterocytes in EV39-treated organoids (Fig. 3b), we estimated the enterocyte maturity score by averaging the expression levels of enterocyte genes that increase with age (Supplementary Table 3). As expected, EV39-treated preterm organoids showed a higher enterocyte maturity score compared to control or EV42-treated organoids (Fig. 3d). Moreover, genes upregulated by EV39 compared to control were enriched for gene ontologies related to the transport of lipids, sterols, and cholesterol (Fig. 3e), similar to metabolic pathways enriched in adult-type (type II) enterocytes (Supplementary Fig. 2g).

Compared to term infants, the small intestinal epithelium of preterm infants exhibits reduced digestive capacities in enterocytes because some digestive enzymes develop during the later stages of gestation[9,68]. Given that significant enterocyte maturation occurs from the fetal stage to adult stage during small intestinal development (Fig. 2a) and that EV39 induced enrichment of adult-like type II enterocytes (Fig. 3b), we investigated whether specific genes related to digestion were altered by EV39. Both EV39 and EV42 altered the expression of genes encoding digestive enzymes, compared to the control, but in a distinct manner (Supplementary Fig. 3h). We thus compared key genes involved in protein digestion, *TMPRSS15* and *ANPEP*, by quantitative Real-Time PCR (qRT-PCR), which were enriched in enterocytes from the pediatric/adult stages (Supplementary Fig. 2i). *TMPRSS15* encodes enteropeptidase, which initiates a protease activation cascade essential for protein digestion, and *ANPEP* encodes alanyl aminopeptidase, which plays a role in the final digestion of peptides generated from hydrolysis of proteins[69,70]. EV39 induced the expression of these genes in two lines of preterm intestinal organoids (Fig. 3f, Supplementary Fig. 3g), suggesting that EV39 might enhance the nutritional value of proteins and peptides by regulating key enzymes involved in their digestion.

In the 3rd trimester of pregnancy, the fetus increases its nutrient demands to support rapid tissue growth and fat deposition; however, preterm birth disrupts the placental transfer of essential nutrients such as fatty acids, exacerbating the nutritional challenges for preterm neonates[71,72]. We therefore investigated whether EV39 induces genes involved in nutrient absorption, including fatty acids, amino acids, and inorganic solutes (Fig. 3g-i, Supplementary Fig. 3h–k).

Among fatty acid transporter genes, EV39 induced the expression of *APOB, ACSL5*, and *SLC27A4* (Fig. 3g, Supplementary Fig. 3g, i), which were also more enriched in the 2nd trimester or pediatric/adult stages than in the 1st trimester stages (Supplementary Fig. 2h). *APOB* (apolipoprotein B) plays a crucial role in lipid transport by serving as an essential structural component of lipoprotein particles, such as chylomicrons, to facilitate the absorption and transport of dietary lipids[73]. During fetal development, the human intestine progressively increases the editing of *APOB* transcripts, enhancing the efficiency of lipid transport to meet the growing energy and developmental needs, coinciding with the onset of intestinal development[74,75]. *ACSL5*, the major small intestinal acyl-coenzyme A (CoA) synthetase, mediates the initial step of dietary fat absorption within enterocytes by adding CoA to fatty acids, forming acyl-CoAs that are effectively trapped inside enterocytes[76]. *SLC27A4* encodes a protein responsible for long-chain fatty acid (LCFA) transport in the small intestine, esterifying long and very long-chain fatty acids with CoA[77].

Among amino acid transporters genes (SLC families: 1, 3, 6, 7, 15, 16, 25, 36, 38, and 43)[78], many genes in the SLC6 and SLC7 families, exhibited elevated expression following EV39 treatment in preterm organoids (Supplementary Fig. 3j). The SLC6 family encodes epithelial neutral amino acid transporters, while the SLC7 family is associated with cationic amino acid and glycoprotein transport[79,80]. Among amino acid transporter genes exhibiting higher expression in the pediatric/adult stages than in the fetal stages (Supplementary Fig. 2l), *SLC6A19*, *SLC25A12*, and *SLC1A1* were also enriched in EV39-treated preterm organoids (Fig. 3h). *SLC6A19* encodes a neutral amino acid transporter, which facilitates the transport of essential amino acids, such as leucine, valine, and methionine[81]. The SLC25 family encodes mitochondrial carriers, and *SLC25A12* specifically encodes the aspartate/glutamate carrier isoform 1 (AGC1). *SLC1A1* encodes an anionic amino acid transporter, which has Na^+-dependent transport activity for aspartate and glutamate[82]. Our findings, which showed that EV39 induces changes in genes involved in protein/peptide digestion (Fig. 3f, Supplementary Fig. 3g) and the absorption of amino acids resulting from digestion (Fig. 3h, Supplementary Fig. 3g), hold potential translational value. This is particularly relevant because preterm infants require higher levels of protein and amino acids than term infants to achieve normal growth[83].

The absorption of nutrients, such as dipeptides, free amino acids and fatty acids, depends on the activity of specific transporters. This process is accompanied by cotransport or reverse transport of inorganic solutes (Na^+, H^+, Cl^-, or HCO_3^-), relying on ion exchangers to create driving forces (transmembrane ion gradients)[84]. Among the genes involved in transporting inorganic solutes, EV39 treatment upregulated Na^+/H^+ exchanger (SLC9A family, NHE), *SLC26A3*, and cystic fibrosis transmembrane conductance regulator (CFTR) channels, which were also enriched in the pediatric/adult stages (Fig. 3i, Supplementary Fig. 2k, 3k). *SLC9A3* (NHE3) is essential for the intestinal absorption of various nutrients and minerals such as Ca^{2+}, glucose, fatty acids, and amino acids[85,86]. *SLC26A3* encodes Cl^-/HCO_3^- exchanger, also known as *DRA*, which is functionally coupled to CFTR in the gastrointestinal tract to mediate Cl^-, HCO_3^-, and fluid secretion[87]. Manifestations of cystic fibrosis, caused by mutations in *CFTR*, and associated complications are linked to maldigestion and malabsorption, potentially affecting nutritional status in the long-term[88]. Thus, the markedly elevated expression of *CFTR* and *SLC26A3* in response to EV39 treatment in two lines of preterm intestinal organoids (Fig. 3i, Supplementary Fig. 3g) could have potential value in improving digestion and nutrient absorption, functions that are often compromised in preterm infants.

Epithelial tight junctions also play a key role in regulating the permeability of ions, nutrients, and water while restricting pathogen entry, thus preserving the epithelial barrier function[89]. We thus investigated whether EV39 affects genes encoding tight junction proteins, such as claudins and zona occludens-1. Similar to their expression increases in the pediatric/adult stages compared to the fetal stage, the expression of claudins (*CLDN1* and *CLDN2*) and zonula occludens-1 (*ZO-1*) in preterm intestinal organoids was increased by EV39 treatment (Fig. 3j, Supplementary Fig. 2m, 3l, 3g). This effect was further validated at the protein level by enhanced ZO-1 staining in EV39-treated preterm intestinal organoids (Supplementary Fig. 3m). Some evidence suggests that *CLDN2* promotes epithelial proliferation[90,91], and EV39 also significantly increased proliferation (Supplementary Fig. 3n). Taken together, our findings demonstrate that MSC-derived EVs, particularly EV39, induce adult-like maturation signatures in two lines of preterm intestinal epithelial models. This encompasses the enrichment of mature enterocyte populations, upregulation of genes involved in digestive enzymes and nutrient transporters, and enhancement of barrier integrity.

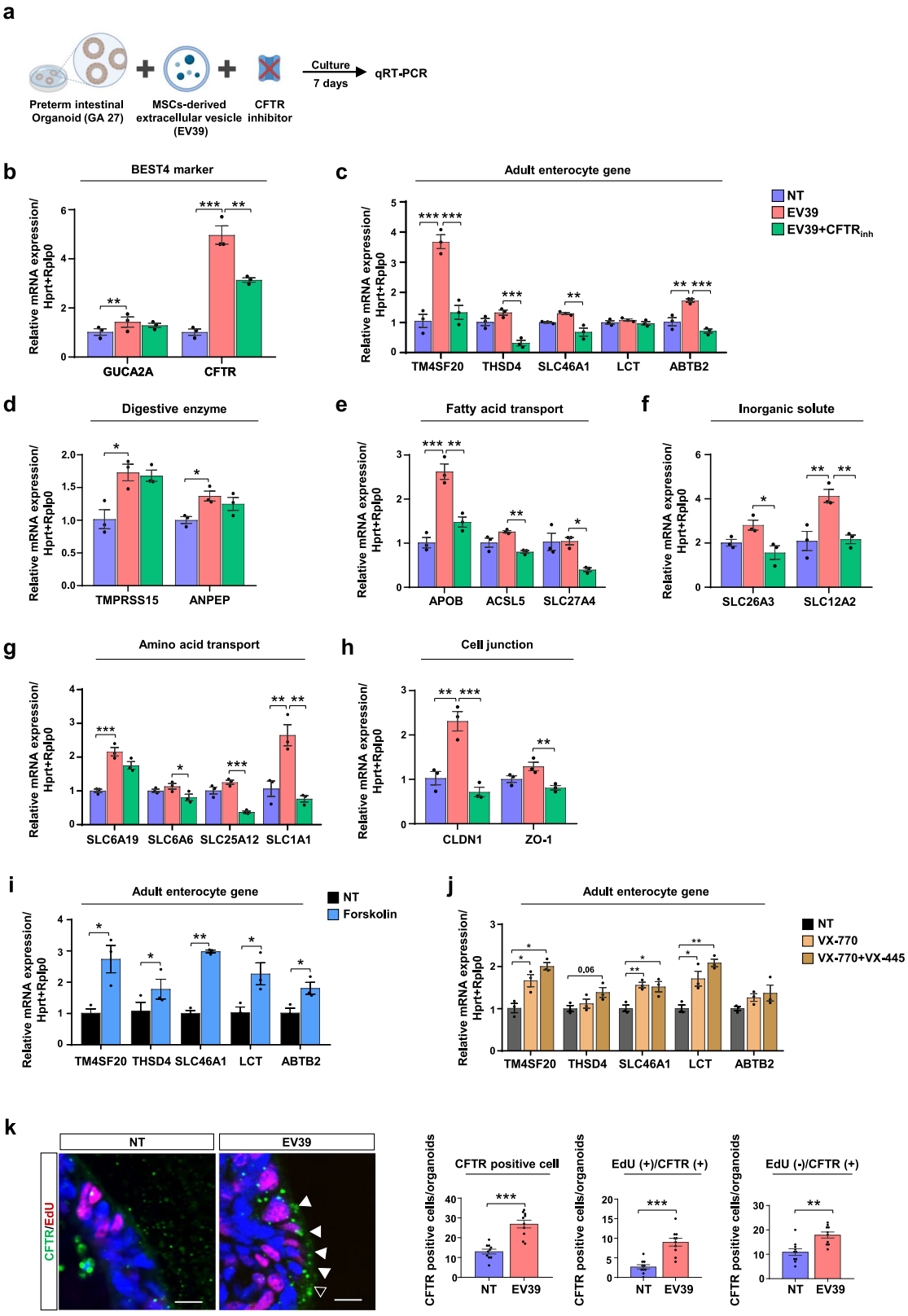

CFTR-dependent enrichment of adult-type enterocyte signatures in mesenchymal stem cell-derived EV39-treated human preterm intestinal epithelial models

EV39 treatment in premature intestinal organoids induced a notable enrichment of BEST4+ enterocytes, which are more abundant in pediatric/adult stages than in fetal stages (Figs. 1d, 3b). Given that the most striking difference between BEST4+ cells in the small intestine versus the colon is *CFTR* expression in the small intestinal BEST4+ cells[21], and our analysis further confirmed previous findings showing enrichment of CFTR High Expresser (CHE) populations in adult-type BEST4+ cells[16,29,62] (Supplementary Fig. 4a, b), we decided to investigate the contribution of CFTR by using a CFTR inhibitor (CFTR inhibitor

Fig. 4 | Mesenchymal stem cell-derived extracellular vesicle (EV39)-induced enterocyte maturation in human preterm intestinal epithelial cells via cystic fibrosis transmembrane conductance regulator (CFTR). a Schematic illustration of the experimental procedure showing preterm intestinal epithelial cells treated with EV39 (2×10^9 EVs/mL) and a cystic fibrosis transmembrane conductance regulator (CFTR) inhibitor (CFTR inhibitor 172, 10 μM) for seven days. Relative mRNA expression of BEST4+ enterocyte marker genes (**b**), adult enterocyte marker gene (**c**), and functional enterocyte markers: digestive enzyme genes (**d**), fatty acid transporter genes (**e**), inorganic solute transporter genes (**f**), amino acid transporter genes (**g**), and cell junction genes (**h**) in preterm intestinal epithelial cells treated with EV39 (2×10^9 EVs/mL), with or without CFTR inhibitor (CFTRinh, 10 μM) for seven days. mRNA levels of each gene are normalized to *HPRT1* and *RPLP0* levels. NT, non-treated group ($n = 3$, 3 wells per group, EV39 vs. NT, or EV39 + CFTR inhibitor). **i** Relative mRNA expression of adult enterocyte marker gene (*TM4SF20, THSD4, SLC46A1, LCT, ABTB2*) in preterm intestinal epithelial cells treated with forskolin (10 μM) for seven days. mRNA levels of each gene are normalized to *HPRT1* and *RPLP0* levels. NT, non-treated group ($n = 3$, 3 wells per group, NT vs. forskolin). **j** Relative mRNA expression of adult enterocyte marker gene (*TM4SF20, THSD4, SLC46A1, LCT, ABTB2*) in preterm intestinal epithelial cells treated with VX-770 (CFTR potentiator, 3 μM), with or without VX-445 (CFTR corrector, 3 μM) for seven days. mRNA levels of each gene are normalized to *HPRT1* and *RPLP0* levels. NT, non-treated group ($n = 3$, 3 wells per group, NT vs. other groups). **k** (left panel) Representative immunofluorescence images showing EdU-stained nuclei of proliferating cells (red) and CFTR expression (green) in preterm intestinal epithelial cells treated with EV39 (2×10^9 EVs/mL) for seven days. All nuclei were counter-stained with Hoechst. (right panel) Quantification of total CFTR-positive cells and the number of EdU-positive versus EdU-negative cells among CFTR-positive cells in the indicated experimental groups. White-filled arrowheads indicate EdU-labeled CFTR-positive cells, and unfilled arrowheads indicate EdU-negative CFTR-positive cells. NT, non-treated group ($n = 10$, comprising 10 organoids from 2 wells per group, NT vs. EV39). Scale bar = 20 μm. Quantitative data are expressed as the mean ± standard error of the mean (S.E.M.). $^*P < 0.05$, $^{**}P < 0.01$, $^{***}P < 0.001$. *P* values were determined by one-way ANOVA with Dunnett's post hoc test (**b–h**, **j**) and unpaired two-tailed Student's *t*tests (**i**, **k**). See also Supplementary Fig. 4, 5.

172) in the EV39-treated premature human intestinal epithelial model (Fig. 4a).

CFTR inhibition suppressed the EV39-induced increase in BEST4+ cell markers, particularly *CFTR*, but not *GUCA2a* (Fig. 4b). Intriguingly, *TM4SF20*, *THSD4*, *SLC46A1*, and *ABTB2*, which we identified as highly enriched genes in adult enterocytes (Fig. 2c, d) and in EV39-treated preterm organoids (Fig. 3c), were CFTR-dependent (Fig. 4c). This prompted us to investigate whether CFTR inhibition also reverses EV39-induced increases in functional genes for digestive capacity and nutrient absorption. Interestingly, genes encoding fatty acid, inorganic solute, amino acid transport, and cell junction proteins were dependent on CFTR activity, except for those involved in protein digestion (*TMPRSS15* and *ANPEP*) (Fig. 4d-h). Treatment with forskolin, a CFTR activator, was sufficient to increase the expression of adult-type enterocyte genes (Fig. 4i), including those encoding fatty acid, inorganic solute, amino acid transporters, as well as cell junction proteins (Supplementary Fig. 4c), similar to those induced by EV39. This finding led us to investigate whether improving CFTR function using drugs prescribed for cystic fibrosis patients, such as the CFTR potentiator VX-770 (Ivacaftor)[92] and the second-generation CFTR corrector VX-445 (Elexacaftor)[93–95], often used in combination with the first-generation CFTR corrector Tezacaftor, could produce similar effects. Combination treatment with VX-770 and VX-445 effectively induced the expression of adult-type enterocyte genes (Fig. 4j), comparable to those induced by EV39 or forskolin. These treatments also increased the expression of genes involved in fatty acid, amino acid, and inorganic solute transport, as well as cell junction proteins, but not genes associated with protein digestion (*TMPRSS15* and *ANPEP*) (Supplementary Fig. 4d). This aligns with the effects of CFTR inhibition on EV39-induced enterocyte functional gene expression (Fig. 4c-h)

Based on the unexpected effects of CFTR activity on genes expressed in enterocytes, we investigated *CFTR* distribution across the small intestinal epithelial cell population. Consistent with previous findings[16,29,62], *CFTR* expression is highest in BEST4+ cells (Supplementary Fig. 5a). However, unlike the minimal expression of *BEST4* in cell types other than BEST4+ cells (Supplementary Fig. 5b), *CFTR* was relatively highly expressed in ISCs, TAs, and adult-type enterocyte precursors (Supplementary Fig. 5a). The absence of *BEST4* in ISCs aligns with the fact that BEST4+ cells are not found in the proliferating crypt zone and are negative for the cell proliferation marker Ki67[96]. *CFTR* expression, in contrast, is known to be highest in crypt cells, with a gradient decreasing towards the villi tips[97–99], consistent with our observations of *CFTR* expression in ISCs (Supplementary Fig. 5a). This suggests that *CFTR* expression varies significantly across different intestinal cell types, with distinct populations—BEST4+ cells with the highest *CFTR* expression and ISCs with relatively high *CFTR* expression.

Previously, *CFTR* expression in adult mouse ISCs has been reported in Sox9 low ISCs, which are enriched with LGR5, showing that CFTR is expressed in crypt-base stem cells where adult ISCs are located and acts as a growth suppressant[100]. This aligns with *CFTR* expression patterns in ISCs in adult stages (ISC II), along with ISC markers *LGR5* and *OLFM4* (Supplementary Fig. 5c–e). In contrast to the well-documented expression and role of CFTR in the adult intestinal epithelium, its expression in the immature fetal intestinal epithelium has not been well studied. Notably, *CFTR* high cells in fetal ISCs did not co-express *LGR5* and *OLFM4*, distinguishing them from *CFTR* high adult ISCs (ISC II) (Supplementary Fig. 5c–e). This discrepancy led us to investigate whether the cell cycle phases of *CFTR* high ISCs differ between adult and fetal stages.

Consistent with previous findings[101], adult-type ISC II cells were enriched in the G1 phase of the cell cycle, and similarly, *LGR5* high fetal-type ISC I cells were mainly in the G1 phase (Supplementary Fig. 5e, f). However, *CFTR* high fetal ISC I cells were enriched in the S phase and showed a strong correlation with PCNA expression (Supplementary Fig. 5d, f, g), a marker for cell proliferation from early G1 to late S phase[102]. Additionally, this aligned with gene expression of S phase-specific signatures (Supplementary Fig. 5g)[103]. Treatment with forskolin, a CFTR activator, significantly increased EdU labeling, which marks the S phase of the cell cycle (Supplementary Fig. 5h), whereas EV39-induced EdU labeling was significantly inhibited by CFTR inhibitor (Supplementary Fig. 5i), suggesting that CFTR activation induces cell proliferation in human premature intestinal epithelial cells, differing from its suppressive role in cell proliferation in the mouse adult intestinal epithelium[100]. To further explore this, we generated mouse intestinal organoids from postnatal day 2 and 8 weeks of age, where neither EV39 nor forskolin affected cell proliferation (Supplementary Fig. 5j, k). These findings collectively suggest that the role of CFTR activation as a promoter of intestinal cell proliferation is specific to the human premature intestine but not likely in the mouse intestine. This raised the question of whether CFTR-expressing cells can be proliferating. Importantly, CFTR-positive proliferating cells (EdU-positive cells among CFTR-positive cells) were significantly induced by EV39 (Fig. 4k), supporting the findings of CFTR high fetal ISC cells in the S phase (Supplementary Fig. 5d, g).

Collectively, these observations suggest that in the immature ISCs, CFTR activation may promote a proliferative state and potentially drives differentiation into mature adult-type enterocyte precursors, subsequently affecting the functional maturation of the intestinal epithelium. However, whether CFTR in the ISCs or BEST4+ cells contribute to the development of adult-type enterocytes requires further validation.

Enrichment of TGFβ1 signaling pathways in mesenchymal stem cell-derived EV39-treated human preterm intestinal epithelial models

To elucidate the molecular mechanisms underlying EV39-mediated maturation in premature intestinal organoids, we performed gene set enrichment analysis (GSEA), identifying TGFβ signaling as the most significantly enriched pathway in EV39-treated organoids (Supplementary

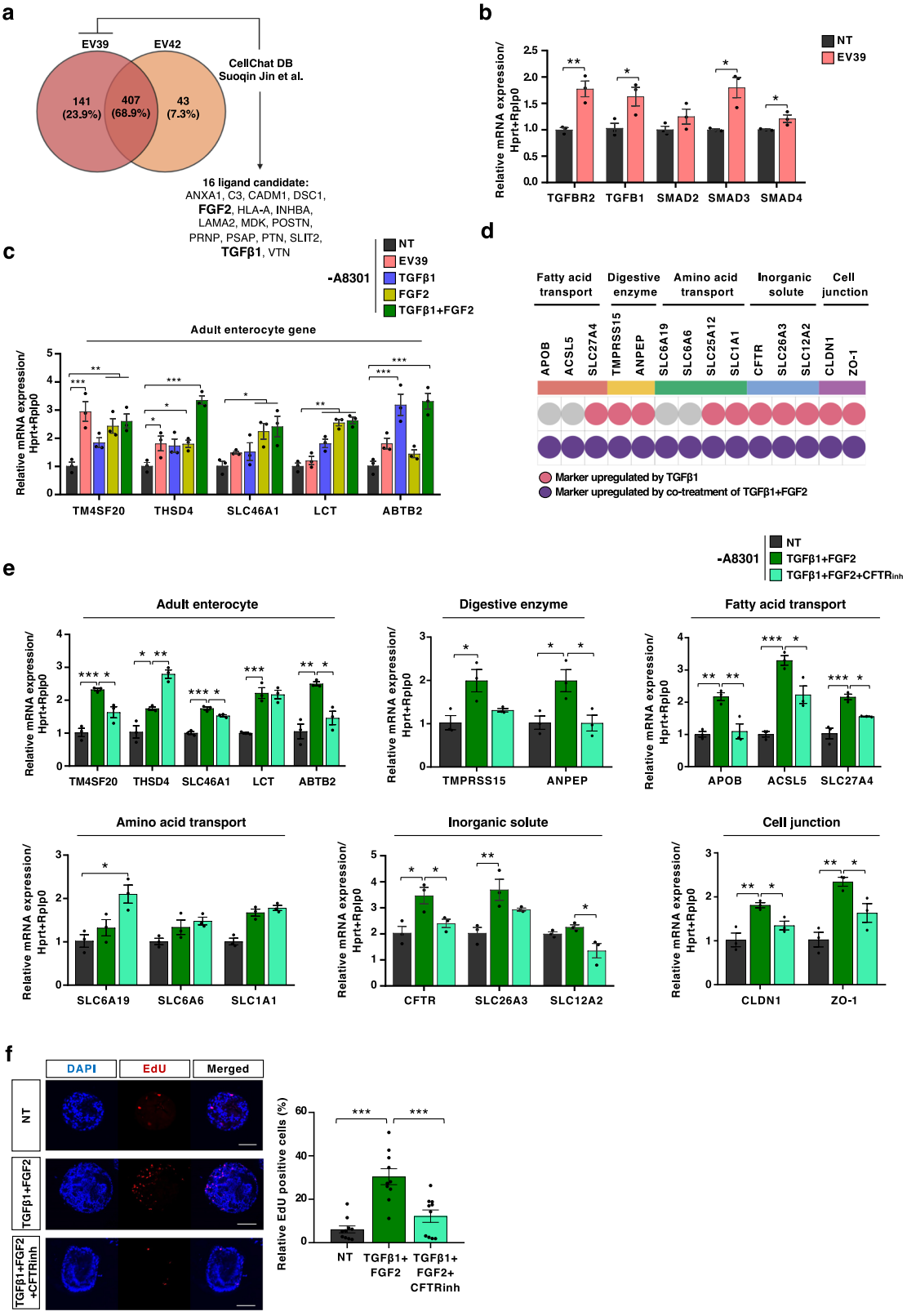

Fig. 6a). Through comprehensive proteomics analysis using liquid-chromatography with tandem mass-spectrometry (LC-MS/MS) on EV39 and EV42 (Supplementary Fig. 6b), we identified 407 common proteins, with 141 unique to EV39 and 43 unique to EV42 (Fig. 5a). To explore cell-cell communication mediators, we focused on ligands and identified 16 ligand candidates using the CellChat v2 database[104], filtering for proteins with more than a twofold increase in EV39 over EV42. These included ANXA1, C3, CADM1, DSC1, FGF2, HLA-A, INHBA, LAMA2, MDK, POSTN, PRNP, PSAP, PTN, SLIT2, TGFβ1, and VTN. The abundance of TGFβ1 in EV39 suggests its role in mediating the enrichment of TGFβ1 signaling pathways by EV39. Quantitative RT-PCR confirmed this, showing EV39-induced increases in *TGFβ1* and downstream effectors such

Fig. 5 | Identification of TGFβ1 and FGF2 as mediators of enterocyte maturation within extracellular vesicle EV39. a Venn diagram of LC-MS/MS-based proteomic analysis of MSCs-derived extracellular vesicles (EV39 and EV42). Among the abundant or unique proteins in EV39, 16 ligand candidates, including fibroblast growth factor II (FGF2) and transforming growth factor I (TGFβ1), were identified based on the CellChat v2 database. **b** Bar plot of relative mRNA expression of TGFβ signaling pathway-associated genes in preterm intestinal epithelial cells treated with EV39 (2×10^9 EVs/mL for seven days) in the presence of a TGFβ1 receptor inhibitor (A83-01, 500 nM, $n = 3$, 3 wells per group, NT vs. EV39). **c** Relative mRNA expression of adult enterocyte marker genes (*TM4SF20, THSD4, SLC46A1, LCT, ABTB2*) in preterm intestinal epithelial cells. The cells were treated with EV39 (2×10^9 EVs/mL), TGFβ1 (0.1 ng/mL), FGF2 (10 ng/mL), or co-treatment of TGFβ1 and FGF2 for seven days, in the absence of A83-01. mRNA levels of each gene are normalized to *HPRT1* and *RPLP0* levels. NT, non-treated group ($n = 3$, 3 wells per group, NT vs. other groups). **d** Summary of gene expression patterns for EV39-induced enterocyte markers, including the effects of TGFβ1 or co-treatment of TGFβ1 and FGF2. **e** Relative mRNA expression of adult enterocyte marker genes and functional enterocyte markers: digestive enzyme genes, fatty acid transporter genes, amino acid transporter genes, inorganic solute transporter genes, and cell junction genes in the preterm intestinal epithelial cells co-treated with TGFβ1 (0.1 ng/mL) and FGF2 (10 ng/mL), with or without CFTR inhibitor (CFTRinh, 10 μM) for seven days. mRNA levels were normalized to *HPRT1* and *RPLP0*. NT, non-treated group ($n = 3$, 3 wells per group, TGFβ1 + FGF2 vs. NT, or TGFβ1 + FGF2 + CFTR inhibitor). **f** (left panel) Representative immunofluorescence images showing the EdU-stained nuclei of proliferating cells (red) in the preterm intestinal epithelial cells co-treated with TGFβ1 (0.1 ng/mL) and FGF2 (10 ng/mL), with or without CFTR inhibitor (CFTRinh, 10 μM) for seven days. All nuclei were counterstained with Hoechst. (right panel) Quantification of EdU-positive cells in the indicated experimental groups. NT, non-treated group ($n = 10$, comprising 10 organoids from 2 wells per group, TGFβ1 + FGF2 vs. NT, or TGFβ1 + FGF2 + CFTR inhibitor). Scale bar = 100 μm. Quantitative data are expressed as the mean ± standard error of the mean (S.E.M.). $^*P < 0.05$, $^{**}P < 0.01$, $^{***}P < 0.001$. *P* values were determined using unpaired two-tailed Student's *t* tests (**b**) and one-way ANOVA with Dunnett's post hoc test (**c**,**e**,**f**). See also Supplementary Fig. 6.

as *SMAD3* and *SMAD4* (Fig. 5b). The induction of *SMADs* via EV39 was notable, given that human intestinal organoid cultures typically require a TGFβ1 receptor inhibitor (A83-01) for long-term maintenance[105]. Our culture conditions for premature intestinal organoids included this inhibitor, but at low concentrations, allowing us to observe TGFβ1 signaling activation even in its presence. We then treated premature intestinal organoids with either EV39 or TGFβ1 in the absence of A83-01. EV39, regardless of the presence of A83-01, induced the expression of genes highly enriched in adult-type enterocytes (Fig. 5c), as well as genes encoding fatty acid, inorganic solute, amino acid transporters, and cell junction proteins—key functions of mature enterocytes (Supplementary Fig. 6d). Most of these genes, including *CFTR*, were regulated by TGFβ1, though not all.

To identify additional factors, we focused on FGF2, which was uniquely present in EV39 (Fig. 5a) and more enriched in pediatric/adult stages than in fetal stages (Supplementary Fig. 6c). While FGF2 did not regulate *CFTR* expression, the combination of TGFβ1 and FGF2 was sufficient to induce the expression of EV39-induced genes in two lines of preterm intestinal organoids (Fig. 5d, Supplementary Fig. 6d, e), indicating that the effects of EV39 are mediated through these ligands. CFTR-dependent regulation of adult-type enterocyte genes was observed following treatment with TGFβ1 and FGF2, similar to the effects of EV39, with the exception of amino acid transporter genes (Fig. 5e). This suggests that CFTR activation mediates downstream effects of these signaling pathways in the premature intestine. As expected, the combination of TGFβ1 and FGF2 also promoted proliferation in preterm organoids to levels comparable to EV39 treatment (Supplementary Fig. 6f), which was similarly dependent on CFTR activity (Fig. 5f). CFTR-dependent cell proliferation by TGFβ1 and FGF2 was also observed in GA24 organoids (Supplementary Fig. 6g). Interestingly, CFTR-high fetal ISC I cells exhibited enriched expression of *TGFBR1*, *TGFBR2*, *FGFR2* and *FGFR4*, along with an S phase signature (Supplementary Fig. 5g, 6h). Co-treatment with TGFβ1 and FGF2 significantly increased the proportion of CFTR-positive proliferating cells (Supplementary Fig. 6i), suggesting that CFTR-high fetal ISC I cells are likely cycling stem cells that mediate TGFβ1 and FGF2 signals to drive proliferation and subsequent enterocyte maturation.

CFTR-dependent functional enterocyte maturation in human premature intestinal epithelial models via EV39 or TGFβ1 and FGF2

To corroborate the EV39- or TGFβ1 and FGF2-induced enrichment of adult-type enterocyte signatures, we investigated whether these treatments improve epithelial barrier integrity and fatty acid uptake in human premature intestinal epithelial models, with a focus on CFTR dependency. To assess epithelial barrier integrity, we cultured 3D premature intestinal organoids as monolayers in transwell inserts, treated them with EV39 or TGFβ1 and FGF2, and then measured the apical-to-basolateral passage of fluorescein isothiocyanate (FITC)-Dextran (4 kDa) across the epithelium. Consistent with the gene expression changes (Figs. 3j, 5e), EV39 or co-treatment with TGFβ1 and FGF2 decreased the fluorescence level of FITC-dextran in the bottom chamber (Fig. 6a). CFTR-dependent enhancement of barrier function by TGFβ1 and FGF2 was observed in two lines of preterm intestinal organoids (Fig. 6b). This finding was further supported by the increased cell junction marker ZO-1 and proteins involved in fatty acid uptake, such as FABP1 (Fig. 6c), which was reversed by CFTR inhibition (Fig. 6d). Finally, long-chain fatty acid uptake was significantly enhanced by EV39 or TGFβ1 and FGF2, as evidenced by the increased intracellular BODIPY-C16 fatty acid fluorescence intensity (Fig. 6e). TGFβ1 and FGF2-induced long-chain fatty acid uptake was also dependent on CFTR activity in two lines of preterm intestinal organoids (Fig. 6f). These finding indicate that EV39 and its key ligands, FGF2 and TGFβ1, promote cell integrity and fatty acid uptake in the human premature intestinal epithelium through CFTR-dependent mechanisms.

Discussion

This study provides significant insights into the developmental dynamics underlying the maturation of the human intestinal epithelium. By integrating scRNA-seq data across fetal, pediatric, and adult stages, we have delineated distinct enterocyte differentiation trajectories, identifying key markers specific to more mature developmental stages. This comprehensive approach allowed us to assess the impact of MSC-derived EVs on human premature intestinal epithelial models, revealing that EV39 significantly enhances the expression of adult-like enterocyte markers and promotes functional maturation in a CFTR-dependent manner. Importantly, we identified TGFβ1 and FGF2 as critical mediators within EV39 that drive these maturation processes.

CFTR (Cystic Fibrosis Transmembrane Conductance Regulator), a key regulator of chloride and bicarbonate secretion[106], is crucial for maintaining ion and fluid homeostasis[107] and facilitating mucin secretion[108]. CFTR dysfunction, as seen in cystic fibrosis (CF), leads to thickened mucus and gastrointestinal pathologies[109]. Our findings expand CFTR's recognized role by demonstrating that its activation enhances adult-type enterocyte gene expression and promotes functional maturation. CFTR modulators, such as Elexacaftor–tezacaftor–ivacaftor, which target the underlying CFTR defect, have shown positive effects on BMI and overall nutritional status in patients aged 12 years or older with cystic fibrosis (CF)[110,111], highlighting the pivotal role of CFTR in preventing these gastrointestinal pathologies.

Meconium-related ileus (MRI) in term infants has traditionally been associated with CF[112]. However, with the increased survival of extremely premature infants, cases of MRI without CF are becoming more common, particularly in regions like East Asia where CF prevalence is low[113,114]. The pathophysiology of MRI without CF is thought to resemble CF-related MRI, with highly tenacious meconium obstructing immature intestines that have compromised ionic secretory function and intestinal motility[115]. As these patients lack CFTR mutations, it is postulated that decreased CFTR activity,

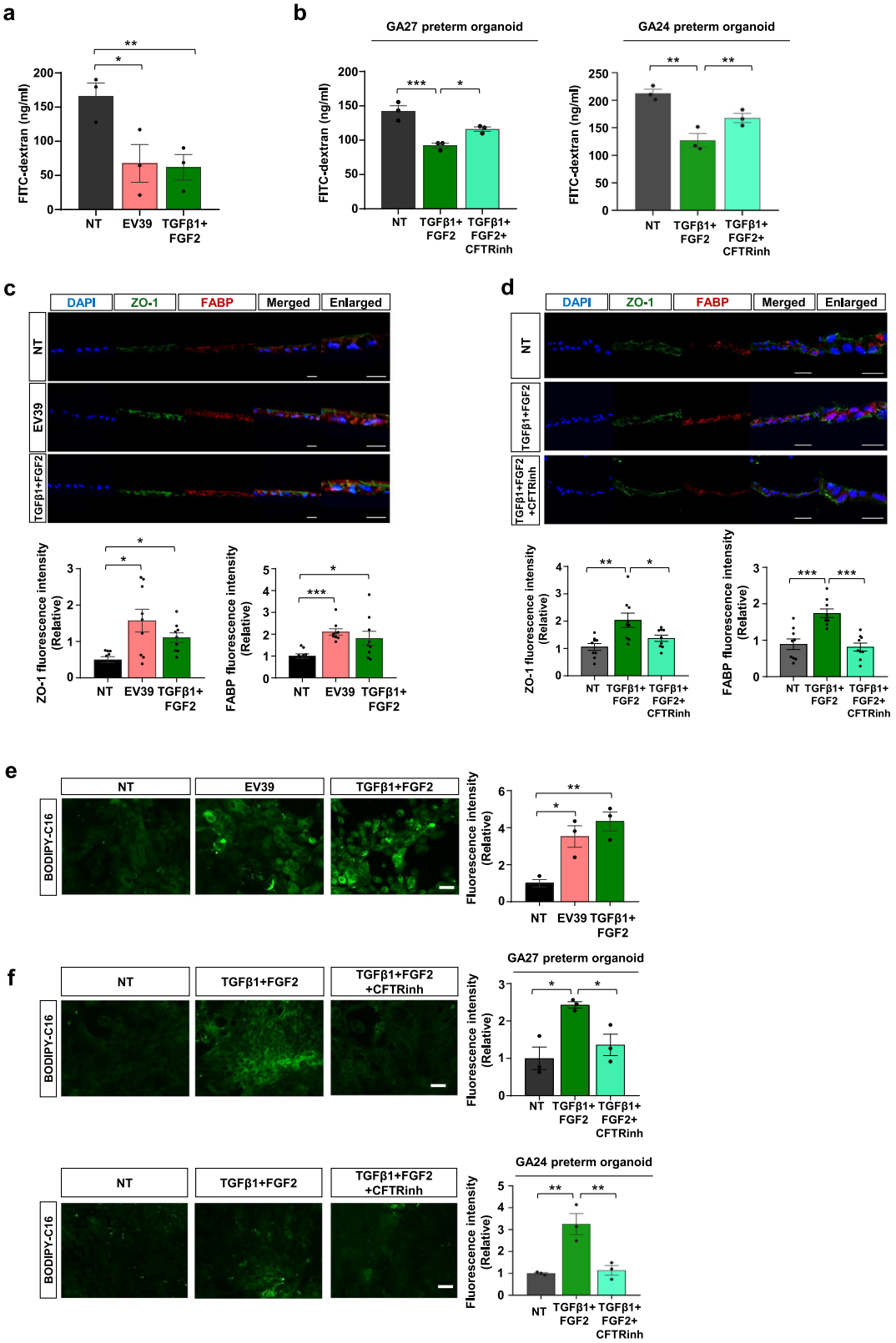

rather than genetic mutations, may be the underlying cause. Cases where CF mothers received CFTR modulators during pregnancy have shown resolution of MRI in their infants[116,117], suggesting a preventative effect on fetal intestinal pathologies[118]. Similarly, pediatric CF patients have shown improvements in gut environment following CFTR modulator administration[116,119]. To validate the relationship between reduced CFTR activity and MRI, future studies should examine CFTR activity in intestinal tissue samples from MRI patients. If confirmed, CFTR modulators could be explored as new preventive and therapeutic strategies for high-risk infants, such as those born prematurely or exposed to antenatal $MgSO_4$, which is often used for fetal neuroprotection but has been associated with an increased the risk of MRI[120]. To the extent of our knowledge, this research

Fig. 6 | CFTR-dependent functional maturation of human preterm intestinal epithelial cells by EV39 or TGFβ1 and FGF2. a Quantification of FITC-dextran fluorescence concentrations in the basolateral well of transwell membranes, measuring leakage from the upper to the lower chambers. The measurement was taken from the lower chamber after treatment with EV39 (2×10^9 EVs/mL) or co-treatment with TGFβ1 (0.1 ng/mL) and FGF2 (10 ng/mL) for eight days. NT, non-treated group ($n = 3$, 3 wells per group, NT vs. other groups). **b** Quantification of FITC-dextran fluorescence concentrations in the basolateral well of transwell membranes, measuring leakage from the upper to the lower chambers. The measurement was taken from the lower chamber after co-treatment with TGFβ1 (0.1 ng/mL) and FGF2 (10 ng/mL), with or without CFTR inhibitor (CFTRinh, 10 μM) in GA 27 (left panel) or GA 24 (right panel) preterm intestinal organoids for eight days. NT, non-treated group ($n = 3$, 3 wells per group, TGFβ1 + FGF2 vs. NT, or TGFβ1 + FGF2 + CFTR inhibitor). c (upper panel) Representative immunofluorescence images showing the tight junction marker zonula occludens-1 (ZO-1, green) and fatty acid uptake marker (FABP1, red) in preterm intestinal epithelial cell layers treated with EV39 (2×10^9 EVs/mL) or co-treated with TGFβ1 (0.1 ng/mL) and FGF2 (10 ng/mL) for eight days. (lower panel) Fluorescence intensity of ZO-1 and FABP1 proteins in the indicated experimental groups. NT, non-treated group ($n = 9$ per sections group, NT vs. other groups). Scale bar = 50 and, 20 μm for enlarged images, respectively. d (upper panel) Representative immunofluorescence images showing the tight junction marker zonula occludens-1 (ZO-1, green) and fatty acid uptake marker (FABP1, red) in preterm intestinal epithelial cell layers co-treated with TGFβ1 (0.1 ng/mL) and FGF2 (10 ng/mL), with or without CFTR inhibitor (CFTRinh, 10 μM) for eight days. (lower panel) Fluorescence intensity of ZO-1 and FABP1 proteins in the indicated experimental groups. NT, non-treated group ($n = 9$ per sections group, TGFβ1 + FGF2 vs. NT, or TGFβ1 + FGF2 + CFTR inhibitor). Scale bar = 50, and 20 μm for enlarged images, respectively. **e** (left panel) Representative immunofluorescence images showing BODIPY-labeled C16:0 in preterm intestinal epithelial cells treated with EV39 (2×10^9 EVs/mL) or co-treated with TGFβ1 (0.1 ng/mL) and FGF2 (10 ng/mL) for eight days. (right panel) Absorption levels of BODIPY-C16 were measured using a microplate reader. NT, non-treated group ($n = 3$, 3 wells per group, NT vs. other groups). Scale bar = 100 μm. f (left panel) Representative immunofluorescence images showing BODIPY-labeled C16:0 in GA 27 (upper panel) or GA 24 (bottom panel) preterm intestinal epithelial cells co-treated with TGFβ1 (0.1 ng/mL) and FGF2 (10 ng/mL), with or without CFTR inhibitor (CFTRinh, 10 μM) for eight days. (right panel) Absorption levels of BODIPY-C16 were measured using a microplate reader. NT, non-treated group ($n = 3$, 3 wells per group, TGFβ1 + FGF2 vs. NT, or TGFβ1 + FGF2 + CFTR inhibitor). Scale bar = 100 μm. Quantitative data are expressed as the mean ± standard error of the mean (S.E.M). $^*P < 0.05$, $^{**}P < 0.01$. *P* values were determined using one-way ANOVA with Dunnett's post hoc test (**a–f**).

may also pave the way for novel treatments for other conditions affecting immature intestine, such as necrotizing enterocolitis (NEC), and address long-term complications in preterm infants, such as extrauterine growth restriction due to suboptimal intestinal absorptive capacity.

Our study also uncovered a population of proliferating CFTR-expressing cells during the early stages of intestinal development. These cells appear to serve as a crucial transitional population, possibly bridging the gap between undifferentiated stem cells and mature enterocytes. The presence of CFTR in proliferating cells suggests a novel function for CFTR beyond its traditional role. Our findings build on the existing knowledge of CFTR's critical role in crypt cells[121,122], proposing a multifaceted function of CFTR in intestinal stem cells (ISCs) that varies depending on the developmental stage. While CFTR has been shown to inhibit cell proliferation in ISCs of adult mice[100,123], our data suggest a more complex role during premature intestinal development. Specifically, CFTR activation with TGFβ1 and FGF2 appears to promote a proliferative state in premature ISCs, potentially driving these cells toward differentiation into mature enterocytes. This raises the possibility that defective CFTR activity could lead to immature enterocytes with impaired nutrient absorption, a hallmark of CFTR mutations[124–128]. Future studies should investigate whether the CFTR-high proliferative population contributes to the expansion of the intestinal epithelium during periods of rapid growth, ensuring sufficient production of mature enterocytes to meet developmental demands. Tracking CFTR-positive ISCs in preterm intestines would also help clarify their role in enterocyte maturation.

Peptide growth factors such as EGF, TGFβ1, HGF, FGF, and IGF are well-documented for their roles in stimulating gastrointestinal cell proliferation and differentiation[129]. Our study emphasizes the roles of FGF2 and TGFβ1 in intestinal maturation. FGF2 has broad developmental functions across various organ systems[130–133], including the gastrointestinal tract[134,135], although its role in intestinal maturation has been underexplored. FGF2 often works in concert with other growth factors, such as TGFβ1 and EGF, to regulate the complex processes of cell growth, differentiation, and tissue formation in the intestine[136]. TGFβ1 is found in developing gastrointestinal tissue[137] and is known to regulate regeneration[138], reconstitution[139], de-differentiation[140], enterocyte proliferation[141], and enterocyte differentiation[142]. The role of TGFβ1 in the crypt-villus axis remains debated, with some studies suggesting that TGFβ1 is elevated in undifferentiated crypt cells[137], while others report its high expression at the differentiated cells located at the villus tip[143]. Additionally, while some studies indicate that TGFβ1 inhibits proliferation and promotes differentiation[141,144], other research suggests that TGFβ1 signaling enhances cellular proliferation in the crypt under irradiation[138]. TGFβ1 also exhibits a protective effect by enhancing intestinal integrity in response to TNFα challenges[145], but TGFβ1-mediated growth factor signaling has been implicated in tumorigenesis in colorectal cancer[146]. These findings highlight the dichotomous functions of TGFβ1 in the intestine.

In summary, our study advances the understanding of the molecular mechanisms underlying intestinal maturation, highlighting CFTR's critical role and the therapeutic potential of targeting CFTR alongside the FGF2 and TGFβ1 signaling axis. Using human preterm intestinal organoids, we demonstrated that CFTR-dependent cell proliferation may be unique to the human premature intestine. However, the study's generalizability is limited by the availability of only two lines of preterm intestinal organoids, owing to challenges in accessing ileal tissue from preterm infants. This constraint highlights the need of future studies utilizing preterm intestinal models derived from infants of varying ages and clinical presentations to address potential inter-individual variability. Despite these limitations, our findings specifically expand the understanding of human intestinal development and suggest potential therapeutic strategies. For instance, CFTR modulators already in clinical use for patients with CFTR dysfunction could be repurposed to enhance intestinal function in preterm infants. Further research is essential to comprehensively evaluate the therapeutic potential of targeting the FGF2 and TGFβ1 signaling axis, which is intricately linked to CFTR activity in the premature human small intestine. Additionally, exploring the complex regulatory networks governing intestinal maturation will be vital for developing innovative therapies to address the challenges of intestinal immaturity in high-risk infants.

Methods

Human preterm intestinal tissues

Human preterm small intestinal tissue was provided by Samsung Medical Center. The study was reviewed and approved by the IRB of Samsung Medical Center (IRB approval number: 2021-06-064) and all methods were performed according to the IRB committee's regulations. All ethical regulations relevant to human research participants were followed. The sample was obtained from the NICU with informed consent from the donor's parents. Terminal ileal tissue from preterm infants born at 24 weeks and 27 weeks gestational age (GA), who underwent ileostomy at a corrected age of 25 weeks and 28 weeks, respectively, were utilized for this study. One preterm infant with a GA of 24 weeks was male and weighed 470 g at birth, while another preterm infant with a GA of 27 weeks was female and weighed 660 g. Both infants presented with bowel ileus and abdominal distension but did not develop necrotizing enterocolitis (NEC). The affected segment was resected, and a double-barrel ileostomy was performed. The resected tissue was sent for pathological diagnosis, which later revealed nonspecific

findings consistent with a hemorrhagic infarct. A portion of the tissue was processed for organoid immediately placed on ice after the surgical removal, minced into approximately 1 mm x 1 mm pieces, and stored in cryopreservation medium CELLBANKER 1 (ZENOGEN PHARMA CO., LTD.; Koriyama, Fukushima, Japan) at −120 °C.

Mice

All animal experiments were conducted in compliance with ethical guidelines approved by the Institutional Animal Care and Use Committee (IACUC) at the POSTECH Biotech Center. Ethical approval for this study was obtained We have complied with all relevant ethical regulations for animal use. Eight-week-old male C57BL/6 N mice (Orient bio, C57BL/6NCrlOri) and postnatal day two mice were used for organoid establishment. The mice were housed in specific-pathogen-free (SPF) conditions with temperature and humidity control (22 ± 3°C and 55 ± 5% humidity) in individually ventilated cages (IVC), with a 12-hour light and 12-hour dark cycle. A standard rodent chow diet and water were provided ad libitum. Euthanasia was performed by carbon dioxide (CO_2) inhalation, following ethical guidelines to minimize distress. Mice were euthanized in their home cage, and a fill rate of 30–70% of the chamber volume per minute with 100% CO_2 was used to achieve a balanced gas mixture and ensure rapid unconsciousness.

Alignment of 10X Genomics scRNA-seq data

Raw sequencing data from 10x Genomics single-cell RNA sequencing (scRNA-seq) gene expression (GEX) were aligned to the 10x Genomics provided Human GRCh38 (GENCODE v32/Ensembl98) reference (2020-A) using the CellRanger count (v7.2.0) with default parameters.

Deconvolution of hashed samples

Multiplexed samples with hashtag oligos (HTOs) from Fawkner-Corbett et al. and Burclaff et al. were demultiplexed as previously described[147]. Initially, each corresponding antibody library was deconvoluted separately using CITE-seq-count (v1.4.5) with the following parameter: -cbf 1 -cbl 16 -umif 17 -umil 28 -T 8 -cells 200000. Note that Burclaff et al.[29] stained single-cells with TotalSeq Anti-Human Hashtag Antibody B as feature barcoding technology, which caused a discrepancy between GEX and HTO. To complement GEX barcodes and HTO barcodes, the cellular barcodes were transformed based on 10x v3 barcode whitelist comprising complete set of unique variants. HTO barcodes present in both GEX and HTO were only selected for demultiplexing step. Filtered UMI count matrices of hashed pool were normalized by log-normalization and then implemented into HTODemux function to demultiplex samples based on HTO enrichment. By performing k-medoid clustering on the normalized HTO values, k (number of samples) +1 clusters were obtained, and some clusters were defined as negative cluster based on the calculated negative distribution for HTO. We fitted a negative binomial distribution to the negative cluster to define threshold at 99th percentile of normalized UMI counts for the hashtag. Negative group and doublet group assigned to either none or multiple hashtags were excluded.

Quality control and processing of scRNA-seq

96 intestinal scRNA-seq data were processed by Seurat package (v5.1.0). Scrublet (v.0.2.3) was applied individually for doublet detection in non-multiplexed samples with automatically determined threshold of doublet score[148]. After confirming co-localization of predicted doublets, they were excluded from downstream analysis. Cells with less than 1000 genes or more than 20,000 genes, and cells with more than 10% (fetus) or 50% (pediatric and adult) of mitochondrial transcripts were considered as ambient RNA or doublet and excluded. Listed ribosomal genes, mitochondrial genes and sex chromosomal genes were removed. Feature counts of each cell were normalized by log-normalization method and 3000 highly variable genes were identified by variance stabilizing transformation method. Linear transformation was applied to normalized expression levels for linear dimensional reduction. Principal component analysis (PCA) was performed based on scale data of highly variable genes. Uniform manifold approximation and projection (UMAP) and Louvain clustering was applied to top 20 PCs to visualize cellular heterogeneity. Batch effect was corrected by using harmony (v1.2.0) algorithm[35]. Harmony based calculation of dimensionality reduction was performed before UMAP calculation and clustering.

Cell type annotation

Highly expressed genes for each cluster were identified using the Preto package, with criteria including AUC > 0.6, log2FC > 0.25, padj <0.05, and pct_in >25. Clusters were manually annotated based on marker gene expression patterns. Clusters that expressed either no marker genes or multiple cell type markers were classified as doublets and excluded from downstream analysis, including the MUC2 + FABP2+ doublets reported by Elmentaite et al.[30]. Additionally, as noted by Yu et al.[34], we identified potentially mis-dissected cells from adjacent tissues, such as colonocyte progenitors in the fetal small intestine samples. All potential doublets were removed, and only correctly annotated intestinal cells were used for further analysis.

Quality-controlled intestinal cells were subdivided into mesenchymal (*DCN* +, *COL6A2* +, *COL3A1* +, *COL1A2* +, *MFAP4* +), epithelial (*EPCAM* +, *CDH1, KRT8* +, *KRT18* +, *FXYD3* +, *PERP* +), immune (*CORO1A* +, *CD53* +, *CD37* +, *PTPRC* +, *LCP1* +, *LAPTM5* +), neural (*ASCL1* +, *PHOX2B* +, *CHRNA3* +, *HAND2* +, *TBX3* +), endothelial (*CDH5* +, *FLT1* +, *CLDN5* +, *EGFL7* +, *ESAM* +, *ECSCR* +), and erythroid (*GYPA* +, *HBM* +, *HBA1* +, *HEMGN* +). Epithelial lineage cells were further subdivided into ISC (*LGR5* +, *OLFM4* +, *ASCL2* +), proximal progenitor (*FGG* +, *FGB* +), TA (*MKI67* +, *TOP2A* +, *PCNA* +), Paneth (*DEFA5* +, *DEFA6* +, *REG3A* +), enterocyte precursor (*FABP2* +, *APOA4-*, *RBP2* +), enterocyte (*FABP2* +, *APOA4* +, *RBP2* +), BEST4 enterocyte (*BEST4* +, *OTOP2* +, *CFTR* +), goblet (*MUC2* +, *CLCA1* +, *TFF3* +), EEC (*CHGA* +, *NEUROD1* +), and tuft (*POU2F3* +, *LRMP* +, *TRPM5* +). Enterocyte were classified into type I (fetal abundant) and type II (adult abundant) based on sample age.

Pseudotime cell analysis and RNA velocity analysis

Single-cell trajectories were constructed using monocle 3 package[40]. Each cell was assigned to a discrete partition which collectively formed distinct trajectories. By fitting principal graph within each partition, trajectory graph was constructed. The root node of trajectory was specified by order_cells function (ISCs in our study) for pseudotime computation. For the analysis of pseudotime-dependent genes in fetal and pediatric/adult stages, differentiation paths were initially isolated, and pseudotemporal genes were identified by measuring multi-directional and multi-dimensional spatial autocorrelation using Moran's I statistics (q-value < 0.01, Moran's I > 0.2). Fetal or pediatric/adult abundant genes were further filtered for the respective pseudotemporal genes.

For the analysis of epithelial cell trajectories in fetal and pediatric/adult stages, RNA velocities of single-cells were estimated based on unspliced and spliced mRNA information using Velocyto[37], and RNA velocities were computed using the scVelo 0.3.2 package[149] implemented in Scanpy 1.9.8. Gene-specific velocities were calculated using stochastic models. Partition-based graph abstraction (PAGA) analysis[38] was conducted with the sc.tl.paga function using a 0.15 threshold.

Differential expression analysis

Due to inflated *p* values in single-cell differential expression analysis, single-cells within each biological replicate were aggregated for pseudobulk differential expression analysis[67]. To identify specific and abundant signatures of adult enterocytes, pseudobulk differential expression analysis was conducted using DESeq2. This analysis revealed 344 significantly upregulated genes. Among these, adult enterocyte-specific genes (with log-transformed expression fold change >3) and abundant genes (with log-transformed expression fold change >1) were defined based on the enterocyte expression pattern. Age-dependent enterocyte signatures were generated by comparing

differentially expressed genes (DEGs) between the first trimester and second trimester, as well as between the second trimester and pediatric/adult stages. For functional analysis, the identified DEGs were subjected to gene set enrichment analysis (GSEA) using the MSigDB v2023.2.Hs collection. Enterocyte functional module scores were computed by averaging the expression levels of the listed genes and subtracting the aggregated expression levels of randomly selected control feature sets.

Preprocessing and analysis of RNA-seq

The raw sequencing reads were trimmed for Illumina adapters using Cutadapt (v4.7), and poor-quality reads were removed with Trim Galore (v0.6.10). Quality-controlled reads were then mapped to the ensemble GRCh38 human reference genome using STAR aligner (v2.7.10b). Transcript quantification was performed using RSEM (v1.3.1). Genes with fewer than 10 counts were excluded from differential expression analysis. Normalized counts were obtained through variance stabilizing transformation (VST). Gene set variation analysis (GSVA) was conducted to quantify single gene set activity based on the normalized counts. Differential expression analysis was performed using DESeq2, with significant differentially expressed genes (DEGs) identified by a Benjamini-Hochberg adjusted p value < 0.05 and used for Gene Ontology (GO) term enrichment analysis. Principal component analysis (PCA) was conducted on pseudobulk scRNA-seq samples after removing batch effects using the removeBatchEffects function from the limma package.

Deconvolution of RNA-seq

Reference-based decomposition was performed using Bisque package[150] to estimate cellular composition from bulk expression data. Epithelial single-cell transcriptomic data were used as reference. Only genes common to both epithelial scRNA-seq dataset and bulk RNA sequencing (RNA-seq) of preterm intestinal organoids treated with MSCs derived EVs-treated were included for deconvolution. The Averages proportions of each cell type across replicates were visualized.

Isolation and characterization of extracellular vesicles from mesenchymal stem cells

Human Wharton's jelly-derived mesenchymal stem cells (WJ-MSCs) from two different donors (lot 39 and lot 42), collected with an informed consent for the study reviewed and approved by the Institutional Review Board (IRB) of Samsung Medical Center (IRB approval number: 2016-07-102-043; Date of approval: 2016-09-20; Approval expiration date: 2025-09-15), were provided by the Good Manufacturing Practice (GMP) Facility of Samsung Medical Center. WJ-MSCs were expanded, cultured, and characterized according to the minimum criteria set by the International Society for Cell Therapy[151] before the isolation of extracellular vesicles (EVs). WJ-MSCs were cultured in minimum essential medium (MEM)-α (Gibco; Grand Island, NY, USA) supplemented with 10% fetal bovine serum (Biowest; Bradenton, FL, USA) and 0.1% gentamycin (Gibco; Grand Island, NY, USA). Research cell banking stored in -120°C at passage 4 was thawed and stabilized. 6000 cells / cm^2 WJ-MSCs were seeded to 175 T flask and the medium was changed every 48 h and passaged every 4 days. The doubling time of WJ-MSCs were confirmed consistent. Surface markers of MSCs were confirmed to be positive for CD90, CD73, and CD105 and negative for CD14, CD45, and HLA-DR (Supplementary Fig. 3a, b). The EV isolation and characterization aligned with the minimal information for the study of extracellular vesicles 2018 checklist[152]. At passage 7, WJ-MSCs were preconditioned with 20 units/mL thrombin (Reyon Pharmaceutical Co, Ltd; Seoul, South Korea) in serum-free minimum essential medium (MEM)-α (Gibco; Grand Island, NY, USA) for 3 h. The condition medium was collected once after the 3 h preconditioning for the EV isolation. There were 36,000 cells / cm^2 WJ-MSCs in the flask at the time of condition medium collection. The condition medium was filtrated through 0.22 μm bottle top vacuum filter system (Corning; Corning, NY, USA) to remove cells and diafiltrated with DPBS (Welgene; Daegu, South Korea) through a tangential flow filtration system (KrosFlo® KR2i, Repligen; Waltham, MA, USA), performing both ultrafiltration and diafiltration. mPES membrane with a 300 kDa cut-off was used to filter out debris and isolate EVs. Approximately 5 L of conditioned medium were used to collect 50 mL of EVs. The collected EVs were analyzed using Nanoparticle Tracking Analysis (NTA, NanoSight NS300; Malvern, Malvern, UK). The mean size of EVs was 133.5 ± 1.2 nm and 131.8 ± 2.8 nm, and the mean concentration was 2.14×10^{10} particles/mL and 1.08×10^{10} particles/mL for EV39 and EV42, respectively (Supplementary Fig. 3c). Surface markers of isolated EVs were confirmed to be positive for TSG101 and FLOT-1, and negative for GM130 (Supplementary Fig. 3d). The EVs were diluted in DPBS to a final concentration of 2×10^{10} particles/mL for both EV39 and EV42. EVs stored at −80 °C for less than 6 months were used in this study, with no cryoprotectant used for storage.

Proteomic analysis of MSCs-derived extracellular vesicles (EVs)

Liquid chromatography with tandem mass spectrometry (LC-MS/MS) was performed by KbioHealth, New Drug Development Center (Cheongju-si, Chungcheongbuk-do, Korea) for comprehensive proteomics analysis of EV39 and EV42. Nano LC and Q-Exactive Plus system (Thermo Scientific; Waltham, MA, USA) were used for chromatographic separation, and each sample of EV39 and EV42 was analyzed in duplicate for reliability. The mobile phase consisted of 0.1% formic acid in water and 0.1% formic acid in 80% acetonitrile. The column used was an EASY-Spray 50 cm × 75 μm PepMap RSLC C18 2 μm (Thermo Scientific; Waltham, MA, USA), and the separation was carried out at 50°C. Data were analyzed using Proteome Discoverer software version 2.4 (Thermo Scientific; Waltham, MA, USA) with the human proteome database (UniProt-proteome_HomoSapiens_73099_FASTA). The analysis was performed with the following parameters: MS accuracy of 10 ppm, MS/MS accuracy of 0.8 Da for HCD, and trypsin digestion allowing up to two missed cleavages. Fixed modification included carbamidomethylation of cysteine (+ 57.0215 Da), and variable modifications included oxidation of methionine (+ 15.9949 Da). To ensure high confidence in the identifications, the false discovery rate (FDR) was set to less than 1% at both the peptide and protein levels. FDR estimation was performed using a target-decoy search strategy, where false positives were calculated by comparing target and decoy matches. Additionally, q-values were used to evaluate the reliability of individual peptide-spectrum matches (PSMs) and protein identifications. A q-value threshold of ≤0.05 was applied to ensure that the probability of false identifications among significant results was less than 5%. For relative quantification, proteins with a fold change less than −2 or greater than +2, along with an adjusted p value corresponding to an FDR of ≤0.05, were considered differentially expressed.

Crypt isolation from human and mouse intestinal samples and organoid culture

Crypt isolation and organoid culture from human intestinal samples were carried out as previously described[153]. The ileal tissue from a preterm neonate born at gestational age (GA) of 27 weeks was further minced into small fragments approximately 1mm3 in size. The fragmented epithelium was washed at least five times with ice-cold PBS and gently rocked in 2.5 mM EDTA in PBS for 1 h at 4 °C on a shaker. The crypt palette was suspended in Matrigel (Corning) on ice. Crypt-laden Matrigel was dispensed onto 48-well culture plates, and following solidification of Matrigel droplets, the crypts were overlaid with the following medium: Advanced Dulbecco's Modified Eagle's Medium/F12 (Thermon Fisher Scientific) supplemented with penicillin/streptomycin, 10 mM HEPES, 2 mM GlutaMAX, 1 × B-27 Supplement (Thermo Fisher Scientific), 10 nM gastrin I (Sigma-Aldrich), 1 mM N-acetylcysteine (Sigma-Aldrich), and the niche factors of 100 ng/mL recombinant mouse Noggin (PeproTech), 50 ng/mL recombinant mouse EGF (Invitrogen), 10% R-spondin1 conditioned medium, 500 nM A83-01 (Tocris), 100 ng/mL human Wnt-3α (R&D system). The medium was replaced every 2–3 days, with passage at a 1:3 ratio every 7 days. To prevent anoikis, 10 μM Y-27632 (Sigma-Aldrich) was added for the first 2 days after passaging.

Mesenchymal stem cell (MSC)-derived extracellular vesicles (EV39 and EV42) were applied to preterm intestinal organoids at a concentration of 2×10^9 EVs/mL, with or without CFTR inhibitor 172 (10 μM), for 7 days. Additionally, preterm intestinal organoids were treated with the CFTR activator forskolin (10 μM) or with CFTR modulators VX-770 (3 μM, potentiator) and VX-445 (3 μM, corrector) for 7 days. To activate TGFβ1 and FGF2 signaling, organoids were treated with 0.1 ng/mL TGFβ1 (R&D system) or 10 ng/mL FGF2 (PeproTech) for 7 days, in the absence of A83-01. The experiment was conducted using organoids derived from various passages (passages 4 to 10).

To generate mouse postnatal intestinal organoids, mouse pups at postnatal day 2 were pooled, resulting in approximately 3 mice per experiment. For adult mice intestinal organoids, the middle part of the small intestine of an 8-weeks old mouse was used. For fetal and adult mice intestinal organoids, small intestine sections of approximately 20 cm were harvested, opened longitudinally, rinsed with cold PBS and incubated in 2.5 mM EDTA at 4 °C for 30 min with gentle shaking. Crypts were released after vigorous shaking in cold PBS and passed through a 70 μM cell strainer (BD Biosciences) for further enrichment. Approximately 100 crypts were embedded in 20 μL Matrigel (Corning) and plated in 48-well plates. Both postnatal and adult organoids were maintained in ENR (EGF, Noggin and R-spondin) medium throughout the experiments as previously described in a 48-well plate[154].

Bulk RNA-seq

RNA was extracted from preterm intestinal organoid using the RNeasy Micro Kit (Qiagen). cDNA synthesis was performed using the TruSeq Stranded Total RNA Library Prep Gold kit, following the instructions in the TruSeq Stranded Total RNA Reference Guide (1000000040499 v00). Libraries were sequenced on the NovaSeq 6000 platform with paired-end 101 bp reads, generating 70 million reads per sample.

Real-time quantitative PCR

Total RNA was extracted from preterm intestinal organoids using the RNeasy Micro Kit (Qiagen) and cDNA was synthesized using a High-Capacity cDNA Reverse Transcription kit according to the manufacturer's protocol (Thermo Fisher Scientific). Real-time PCR was performed using the QGreenBlue Master Mix (Low ROX) (Cellsafe, QBLR) with the primers listed in Supplementary Table 4. Samples were normalized to *HPRT1* and *RPLP0*.

Proliferation assay

To assess cell proliferation, the Click-iT® EdU Imaging Kit (Invitrogen, Thermo Fisher Scientific) was used. Human and mice intestinal organoids cultivated in expansion and refined media were incubated with 5-ethynyl-2'deoxyuridine (EdU) at a final concentration of 10 μM for 30 min at 37 °C and then fixed with 4% PFA for 2 h at room temperature. The staining procedure was carried out according to manufacturer's instructions. DNA was counterstained using 4′,6-Diamidine-2-phenylindole dihydrochloride (DAPI, Sigma-Aldrich).

Intestinal epithelial monolayer culture from human intestinal organoids

For generation single-cell suspensions from preterm intestinal organoids, organoids on day seven post-seeding were collected in a 15 mL tube and repeatedly triturated to disrupt the Matrigel. The sample was centrifuged at 3000 rpm for 6 min, and the media and most of the pelleted Matrigel were aspirated. Single-cell suspensions were generated by resuspending the organoid pellets in 500 μL of accutase (Promega) per 1.5 mL low-binding tube and incubated at 37 °C for 10 min. Then, 500 μL of 10% FBS in PBS was added to each tube, and cells were centrifuged at 3000 rpm for 5 min. Cells were counted and resuspended in proliferation media at a concentration of 100,000 cells per well for 24-well transwells (Corning), and 150,000 cells per 48-well plates. Cells were added to the apical chamber of 1% Matrigel-coated transwells in 100 μL of proliferation media for the 24-well transwells or to the 5% Matrigel-coated well in 250 μL proliferation media for 48-well plates.

Fatty acid uptake assay

The fatty acid uptake was evaluated using intracellular BODIPY-labeled fatty acid, as previously described[155]. Briefly, fully differentiated monolayers (day eight post-seeding) were starved in FBS-free medium for 1 h before measurement. BODIPY-FA (BODIPY FL C16, GLP-bio), preincubated with fatty acid/bovine serum albumin (BSA), was then added to the cells and incubated for 6 h at 37 °C in the dark. Media from the apical compartment was removed, and the cells were carefully washed four times with PBS, and the lysed with 5% IGEPAL (Sigma-Aldrich) in water. Afterward, the cell lysates were centrifuged for 1 min at 8000 rpm and BODIPY fluorescence was measured in supernatants. Intracellular fluorescence was measured using a Bio Tek Synergy HTX plate reader following excitation at 485 nm and emission at 528 nm. Fatty acid uptake differences were compared based on relative fluorescence.

In vitro intestinal permeability assay

Permeability assay with fluorescein isothiocyanate (FITC)-Dextran 4 kDa (Sigma) in the 2D intestinal models were performed on day eight. The culture medium was removed from both sides of the Transwell® inserts and washed twice with pre-warmed Hank's Balanced Salt Solution (HBSS). After washing, 750 μL of HBSS was added to the basolateral side and 200 μL of HBSS to the apical side of the inserts. The HBSS on the apical side was replaced with 100 μL of 4 kDa FITC-dextran (FD4, 1 mg/mL). The transwell plates were incubate at 37 °C for 30 min, and then the concentration of FD4 in the basolateral chamber was measured at an excitation wavelength of 480 nm and an emission wavelength of 520 nm, according to the standard curve. The standard curve was established using FD4 concentration of 0, 50, 100, 150, 200, 250, and 300 ng/mL.

Cross-sectional staining

A fully differentiated intestinal monolayer was used for immunofluorescence imaging of functional enterocyte markers (FABP1 and ZO-1, 1:100). The culture medium was removed from both the apical and basolateral chambers, and the transwell membrane was washed with PBS to remove excess media. Then, the transwell membrane was fixed by adding 4% paraformaldehyde PFA to both chambers for 30 min at 25 °C, followed by washing and cryopreservation the membrane with a series of sucrose solution (10% to 30%). To isolate the membrane, a blade scalpel was used to carefully cut the transwell membrane from the well around the edge to detach it from the plastic. Subsequently, the membrane was embedded in optimal cutting temperature (O.C.T.) compound (Sakura Finetek, Tokyo, Japan) in an appropriately sized embedding mold and freeze it on dry ice. For vertical sections, the frozen blocks were cut into 10 μm thick sections using a cryostat microtome at −30 °C. For immunofluorescence analysis, permeabilize the cells with PBS containing 0.1% Triton X-100 and blocked with a 4% BSA solution.

Immunofluorescence microscopy

For the detection of markers of functional enterocytes (CFTR and FABP1, 1:100) or tight junction proteins (ZO-1, 1:100), fully differentiated organoid or organoid-derived monolayer cultures grown in 8-well chambers or 24-well transwells were fixed using 4% paraformaldehyde (PFA), permeabilized with 0.1% Triton X-100, and blocked with 3% BSA. Organoid or monolayers were then incubated overnight at 4 °Cwith primary antibodies for CFTR (Merk, MAB3480), ZO-1 (Invitrogen, 40-2200) and FABP (Abcam, ab7366), followed by secondary antibody staining at room temperature for 2 h. The samples were incubated with Hoechst 33432 (Sigma-aldrich) for 15 min, followed by washing with 1× PBS to stain cell nuclei. Finally, the samples were mounted onto slides using mounting media (ProLong Gold, Invitrogen) and microscopy was performed with a Nikon Ti2-E & CSU-W1 confocal microscope using a 20x objective lens. Image J was used to count CFTR-positive cells and measure fluorescence intensity.

Statistics and reproducibility

The Wilcoxon rank-sum test was employed for non-parametric statistical analysis. The Wald test was applied to evaluate the significance of log2 fold changes for each gene, and P value correction was performed using the Benjamini-Hochberg (BH) method in small intestinal datasets. Quantitative experimental data are expressed as the mean ± standard error of the mean (S.E.M). Statistical significance was assessed using analysis of variance (ANOVA) with Dunnett's post hoc test for comparisons involving more than three groups, and an unpaired two-tailed Student's t test for comparisons between two groups. Results were considered statistically significant at $P < 0.05$. Reproducibility was established by performing all experiments with a minimum of three independent biological replicates, each representing an independent sample derived from an experimental batch. Specific details regarding sample sizes and the number of replicates for each experiment are outlined in the respective figure legends.

Contact for reagent and resource sharing

Further information and requests for resources and reagents should be directed to and fulfilled by Se In Sung (sein.sung@samsung.com), Yun Sil Chang (cys.chang@samsung.com), and Ara Koh (ara.koh@postech.ac.kr).

Reporting summary

Further information on research design is available in the Nature Portfolio Reporting Summary linked to this article.

Data availability

Raw sequencing data for fetal and adult epithelial analyses are available at Array Express (https://www.ebi.ac.uk/arrayexpress) under accession numbers E-MTAB-10187, E-MTAB-8901, E-MTAB-9363, E-MTAB-9489, E-MTAB-9536, and E-MTAB-9543, as well as at GEO under accession numbers GSE158702, GSE158703, GSE158704, GSE158705, GSE158706, GSE158707, GSE158708, GSE158709, GSE158710, GSE158711, GSE158712, GSE158713, GSE158714, and GSE185224. Raw and processed sequencing data for MSC-derived extracellular vesicles (EVs) treated with preterm intestinal organoids are available at GEO under accession number GSE276831. Source data for figures are available in the Supplementary Data.

Received: 16 October 2024; Accepted: 17 March 2025;
Published online: 02 April 2025

References

1. Kong, S., Zhang, Y.H. & Zhang, W. Regulation of intestinal epithelial cells properties and functions by amino acids. *BioMed. Res. Int.* **2018**, 1–10 (2018).
2. Frazer, L.C. & Good, M. Intestinal epithelium in early life. *Mucosal Immunol.* **15**, 1181–1187 (2022).
3. Doyle, L.W. & Anderson, P.J. Adult outcome of extremely preterm infants. *Pediatrics* **126**, 342–351 (2010).
4. Larsen, M.L. et al. The effect of gestational age on major neurodevelopmental disorders in preterm infants. *Pediatr. Res.* **91**, 1906–1912 (2022).
5. Nanthakumar, N. et al. The mechanism of excessive intestinal inflammation in necrotizing enterocolitis: an immature innate immune response. *PloS One* **6**, e17776 (2011).
6. Quinn, J.-A. et al. Preterm birth: Case definition & guidelines for data collection, analysis, and presentation of immunisation safety data. *Vaccine* **34**, 6047–6056 (2016).
7. Howson, C., Kinney, M. & Lawn, J. Born too soon: the global action report on preterm birth. March of Dimes, PMNCH, Save the Children. *World Health Organization* (2012).
8. Berseth, C.L. Gastrointestinal motility in the neonate. *Clin. Perinatol.* **23**, 179–190 (1996).
9. Commare, C.E. & Tappenden, K.A. Development of the infant intestine: implications for nutrition support. *Nutr. Clin. Pract.* **22**, 159–173 (2007).
10. Henderickx, J. G. E., Zwittink, R. D., Van Lingen, R. A., Knol, J. & Belzer, C. The Preterm Gut Microbiota: An Inconspicuous Challenge in Nutritional Neonatal Care. *Front. Cellular Infect. Microbiol.* **9** https://doi.org/10.3389/fcimb.2019.00085 (2019).
11. Indrio, F., Riezzo, G., Cavallo, L., Mauro, A.D. & Francavilla, R. Physiological basis of food intolerance in VLBW. *J. Matern.-Fetal Neonatal Med.* **24**, 64–66 (2011).
12. Neu, J. Gastrointestinal development and meeting the nutritional needs of premature infants. *Am. J. Clin. Nutr.* **85**, 629S–634S (2007).
13. Collado, M.C. et al. Factors influencing gastrointestinal tract and microbiota immune interaction in preterm infants. *Pediatr. Res.* **77**, 726–731 (2015).
14. McCracken, V.J. & Lorenz, R.G. The gastrointestinal ecosystem: a precarious alliance among epithelium, immunity and microbiota. Microreview. *Cell. Microbiol.* **3**, 1–11 (2001).
15. Drozdowski, L.A., Clandinin, T. & Thomson, A.B. Ontogeny, growth and development of the small intestine: Understanding pediatric gastroenterology. *World J. Gastroenterol.* **16**, 787–799 (2010).
16. Elmentaite, R. et al. Cells of the human intestinal tract mapped across space and time. *Nature* **597**, 250–255 (2021).
17. Yilmaz, [.[._._._.].].O.u.m.l.;H. et al. mTORC1 in the Paneth cell niche couples intestinal stem-cell function to calorie intake. *Nature* **486**, 490–495 (2012).
18. Mei, X., Gu, M. & Li, M. Plasticity of Paneth cells and their ability to regulate intestinal stem cells. *Stem Cell Res. Ther.* **11**, 349 (2020).
19. Cunliffe, R. & Mahida, Y. Expression and regulation of antimicrobial peptides in the gastrointestinal tract. *J. Leucoc. Biol.* **75**, 49–58 (2004).
20. Jones, D.E. & Bevins, C.L. Paneth cells of the human small intestine express an antimicrobial peptide gene. *J. Biol. Chem.* **267**, 23216–23225 (1992).
21. Malonga, T., Vialaneix, N. & Beaumont, M. BEST4+ cells in the intestinal epithelium. *Am. J. Physiol.-Cell Physiol.* **326**, C1345–C1352 (2024).
22. Kolf, C.M., Cho, E. & Tuan, R.S. Mesenchymal stromal cells: biology of adult mesenchymal stem cells: regulation of niche, self-renewal and differentiation. *Arthritis Res. Ther.* **9**, 1–10 (2007).
23. Sarugaser, R., Hanoun, L., Keating, A., Stanford, W.L. & Davies, J.E. Human mesenchymal stem cells self-renew and differentiate according to a deterministic hierarchy. *PloS one* **4**, e6498 (2009).
24. Delavogia, E. et al. Mesenchymal stromal/stem cell extracellular vesicles and perinatal injury: One formula for many diseases. *Stem Cells* **40**, 991–1007 (2022).
25. Phinney, D.G. & Pittenger, M.F. Concise review: MSC-derived exosomes for cell-free therapy. *Stem cells* **35**, 851–858 (2017).
26. Rani, S., Ryan, A.E., Griffin, M.D. & Ritter, T. Mesenchymal stem cell-derived extracellular vesicles: toward cell-free therapeutic applications. *Mol. Ther.* **23**, 812–823 (2015).
27. Childs, C.J. et al. EPIREGULIN creates a developmental niche for spatially organized human intestinal enteroids. *JCI Insight* **8**, e165566 (2023).
28. Triana, S. et al. Single-cell transcriptomics reveals immune response of intestinal cell types to viral infection. *Mol. Syst. Biol.* **17**, e9833. (2021).
29. Burclaff, J. et al. A Proximal-to-Distal Survey of Healthy Adult Human Small Intestine and Colon Epithelium by Single-Cell Transcriptomics. *Cell. Mol. Gastroenterol. Hepatol.* **13**, 1554–1589 (2022).
30. Elmentaite, R. et al. Single-cell sequencing of developing human gut reveals transcriptional links to childhood Crohn's disease. *Dev. Cell* **55**, 771–783.e775 (2020).

31. Fawkner-Corbett, D. et al. Spatiotemporal analysis of human intestinal development at single-cell resolution. *Cell* **184**, 810–826.e823 (2021).
32. Holloway, E.M. et al. Mapping Development of the Human Intestinal Niche at Single-Cell Resolution. *Cell Stem Cell* **28**, 568–580.e564 (2021).
33. Holloway, E.M. et al. Differentiation of Human Intestinal Organoids with Endogenous Vascular Endothelial Cells. *Dev. Cell* **54**, 516–528.e517 (2020).
34. Yu, Q. et al. Charting human development using a multi-endodermal organ atlas and organoid models. *Cell* **184**, 3281–3298.e3222 (2021).
35. Korsunsky, I. et al. Fast, sensitive and accurate integration of single-cell data with Harmony. *Nat. Methods* **16**, 1289–1296 (2019).
36. Butler, A., Hoffman, P., Smibert, P., Papalexi, E. & Satija, R. Integrating single-cell transcriptomic data across different conditions, technologies, and species. *Nat. Biotechnol.* **36**, 411–420 (2018).
37. La Manno, G. et al. RNA velocity of single cells. *Nature* **560**, 494–498 (2018).
38. Wolf, F.A. et al. PAGA: graph abstraction reconciles clustering with trajectory inference through a topology preserving map of single cells. *Genome Biol.* **20**, (2019). 59.
39. Fordham, R.P. et al. Transplantation of expanded fetal intestinal progenitors contributes to colon regeneration after injury. *Cell Stem Cell* **13**, 734–744 (2013).
40. Cao, J. et al. The single-cell transcriptional landscape of mammalian organogenesis. *Nature* **566**, 496–502 (2019).
41. Finkbeiner, S.R. et al. Transcriptome-wide analysis reveals hallmarks of human intestine development and maturation in vitro and in vivo. *Stem Cell Rep.* **4**, 1140–1155 (2015).
42. Johnson, T.N., Tanner, M.S., Taylor, C.J. & Tucker, G.T. Enterocytic CYP3A4 in a paediatric population: Developmental changes and the effect of coeliac disease and cystic fibrosis. *Br. J. Clin. Pharm.* **51**, 451–460 (2001).
43. Chen, C., Yin, Y., Tu, Q. & Yang, H. Glucose and amino acid in enterocyte: absorption, metabolism and maturation. *Front Biosci. (Landmark Ed.)* **23**, 1721–1739 (2018).
44. Cosovanu, C. et al. Intestinal epithelial c-Maf expression determines enterocyte differentiation and nutrient uptake in mice. *J. Exp. Med.* **219**, e20220233 (2022).
45. Pettersen, I.K.N. et al. Upregulated PDK4 expression is a sensitive marker of increased fatty acid oxidation. *Mitochondrion* **49**, 97–110 (2019).
46. Stojanović, O. et al. Dietary excess regulates absorption and surface of gut epithelium through intestinal PPARα. *Nat. Commun.* **12**, (2021). 7031.
47. Xu, D. et al. The gluconeogenic enzyme PCK1 phosphorylates INSIG1/2 for lipogenesis. *Nature* **580**, 530–535 (2020).
48. D'Elia, E. et al. Neprilysin inhibition in heart failure: Mechanisms and substrates beyond modulating natriuretic peptides. *Eur. J. Heart Fail.* **19**, 710–717 (2017).
49. Trebbien, R. et al. Neutral endopeptidase 24.11 is important for the degradation of both endogenous and exogenous glucagon in anesthetized pigs. *Am. J. Physiol.-Endocrinol. Metab.* **287**, E431–E438 (2004).
50. Willard, J.R., Barrow, B.M. & Zraika, S. Improved glycaemia in high-fat-fed neprilysin-deficient mice is associated with reduced DPP-4 activity and increased active GLP-1 levels. *Diabetologia* **60**, 701–708 (2017).
51. Bunnett, N.W. et al. Distribution and abundance of neutral endopeptidase (EC 3.4.24.11) in the alimentary tract of the rat. *Am. J. Physiol.-Gastrointest. Liver Physiol.* **264**, G497–G508 (1993).
52. Hickey, J.W. et al. Organization of the human intestine at single-cell resolution. *Nature* **619**, 572–584 (2023).
53. Krege, J.H. et al. Male–female differences in fertility and blood pressure in ACE-deficient mice. *Nature* **375**, 146–148 (1995).
54. Haxhija, E.Q. et al. Modulation of mouse intestinal epithelial cell turnover in the absence of angiotensin converting enzyme. *Am. J. Physiol.-Gastrointest. Liver Physiol.* **295**, G88–G98 (2008).
55. Wong, T.P., Debnam, E.S. & Leung, P.S. Involvement of an enterocyte renin-angiotensin system in the local control of SGLT1-dependent glucose uptake across the rat small intestinal brush border membrane. *J. Physiol.* **584**, 613–623 (2007).
56. Huang, L. et al. Small intestine-specific knockout of CIDEc improves obesity and hepatic steatosis by inhibiting synthesis of phosphatidic acid. *Int. J. Biol. Sci.* **18**, 5740–5752 (2022).
57. Fremder, M. et al. A transepithelial pathway delivers succinate to macrophages, thus perpetuating their pro-inflammatory metabolic state. *Cell Rep.* **36**, 109521 (2021).
58. Laftah, A.H. et al. Haem and folate transport by proton-coupled folate transporter/haem carrier protein 1 (SLC46A1). *Br. J. Nutr.* **101**, 1150–1156 (2008).
59. Urquhart, B.L. et al. The human proton-coupled folate transporter (hPCFT): modulation of intestinal expression and function by drugs. *Am. J. Physiol.-Gastrointest. Liver Physiol.* **298**, G248–G254 (2010).
60. Ishibashi, K., Suzuki, M., Sasaki, S. & Imai, M. Identification of a new multigene four-transmembrane family (MS4A) related to CD20, HTm4 and β subunit of the high-affinity IgE receptor. *Gene* **264**, 87–93 (2001).
61. Uhlén, M. et al. Tissue-based map of the human proteome. *Science* **347**, (2015). 1260419.
62. Busslinger, G.A. et al. Human gastrointestinal epithelia of the esophagus, stomach, and duodenum resolved at single-cell resolution. *Cell Rep.* **34**, (2021). 108819.
63. Cao, J. et al. A human cell atlas of fetal gene expression. *Science* **370**, eaba7721 (2020).
64. Sung, D.K., Chang, Y.S., Sung, S.I., Ahn, S.Y. & Park, W.S. Thrombin preconditioning of extracellular vesicles derived from mesenchymal stem cells accelerates cutaneous wound healing by boosting their biogenesis and enriching cargo content. *J. Clin. Med.* **8**, 533 (2019).
65. Sung, D.K., Sung, S.I., Ahn, S.Y., Chang, Y.S. & Park, W.S. Thrombin preconditioning boosts biogenesis of extracellular vesicles from mesenchymal stem cells and enriches their cargo contents via protease-activated receptor-mediated signaling pathways. *Int. J. Mol. Sci.* **20**, 2899 (2019).
66. Bang, Y. et al. Therapeutic efficacy of thrombin-preconditioned mesenchymal stromal cell-derived extracellular vesicles on Escherichia coli-induced acute lung injury in mice. *Respiratory Res.* **25**, (2024). 303.
67. Squair, J.W. et al. Confronting false discoveries in single-cell differential expression. *Nat. Commun.* **12**, (2021). 5692.
68. Demers-Mathieu, V., Qu, Y., Underwood, M.A., Borghese, R. & Dallas, D.C. Premature infants have lower gastric digestion capacity for human milk proteins than term infants. *J. Pediatr. Gastroenterol. Nutr.* **66**, 816–821 (2018).
69. Kitamoto, Y., Yuan, X., Wu, Q., McCourt, D.W. & Sadler, J.E. Enterokinase, the initiator of intestinal digestion, is a mosaic protease composed of a distinctive assortment of domains. *Proc. Natl. Acad. Sci.* **91**, 7588–7592 (1994).
70. Kruse, T.A. et al. Assignment of the human aminopeptidase N (peptidase E) gene to chromosome 15q13-qter. *FEBS Lett.* **239**, 305–308 (1988).
71. Alshaikh, B.N., Reyes Loredo, A., Knauff, M., Momin, S. & Moossavi, S. The role of dietary fats in the development and prevention of necrotizing enterocolitis. *Nutrients* **14**, 145 (2021).
72. Cetin, I., Alvino, G. & Cardellicchio, M. Long chain fatty acids and dietary fats in fetal nutrition. *J. Physiol.* **587**, 3441–3451 (2009).
73. Sirwi, A. & Hussain, M.M. Lipid transfer proteins in the assembly of apoB-containing lipoproteins. *J. Lipid Res.* **59**, 1094–1102 (2018).

74. Patterson, A.P. et al. Developmental regulation of apolipoprotein B mRNA editing is an autonomous function of small intestine involving homeobox gene Cdx1. *J. Biol. Chem.* **278**, 7600–7606 (2003).
75. Fourati, S. et al. Circulating Apolipoprotein B-48 as a Biomarker of Parenteral Nutrition Dependence in Adult Patients with Short Bowel Syndrome. *Nutrients* **15**, 3982 (2023).
76. Griffin, J.D., Zhu, Y., Reeves, A., Buhman, K.K. & Greenberg, A.S. Intestinal Acyl-CoA synthetase 5 (ACSL5) deficiency potentiates postprandial GLP-1 & PYY secretion, reduces food intake, and protects against diet-induced obesity. *Mol. Metab.* **83**, 101918 (2024).
77. Anderson, C.M. & Stahl, A. SLC27 fatty acid transport proteins. *Mol. Asp. Med.* **34**, 516–528 (2013).
78. Bröer, S. & Fairweather, S.J. Amino acid transport across the mammalian intestine. *Compr. Physiol.* **9**, 343–373 (2018).
79. Bröer, S. The SLC6 orphans are forming a family of amino acid transporters. *Neurochem. Int.* **48**, 559–567 (2006).
80. Jungnickel, K.E., Parker, J.L. & Newstead, S. Structural basis for amino acid transport by the CAT family of SLC7 transporters. *Nat. Commun.* **9**, 550 (2018).
81. Bröer, S. The role of the neutral amino acid transporter B0AT1 (SLC6A19) in Hartnup disorder and protein nutrition. *IUBMB Life* **61**, 591–599 (2009).
82. Kanai, Y. & Hediger, M.A. Primary structure and functional characterization of a high-affinity glutamate transporter. *Nature* **360**, 467–471 (1992).
83. Rozé, J.-C. et al. Association between early amino acid intake and full-scale IQ at age 5 years among infants born at less than 30 weeks' gestation. *JAMA Netw. open* **4**, e2135452 (2021).
84. Lu, X. et al. Ion channels and transporters regulate nutrient absorption in health and disease. *J. Cell. Mol. Med.* **27**, 2631–2642 (2023).
85. Rievaj, J., Pan, W., Cordat, E. & Todd Alexander, R. The Na+/H+ exchanger isoform 3 is required for active paracellular and transcellular Ca2+ transport across murine cecum. *Am. J. Physiol.-Gastrointest. Liver Physiol.* **305**, G303–G313 (2013).
86. Thammayon, N. et al. Na+/H+ exchanger 3 inhibitor diminishes the amino-acid-enhanced transepithelial calcium transport across the rat duodenum. *Amino acids* **49**, 725–734 (2017).
87. Ko, S.B. et al. Gating of CFTR by the STAS domain of SLC26 transporters. *Nat. Cell Biol.* **6**, 343–350 (2004).
88. Li, L. & Somerset, S. Digestive system dysfunction in cystic fibrosis: Challenges for nutrition therapy. *Digestive Liver Dis.* **46**, 865–874 (2014).
89. Ulluwishewa, D. et al. Regulation of tight junction permeability by intestinal bacteria and dietary components1, 2. *J. Nutr.* **141**, 769–776 (2011).
90. Ahmad, R. et al. Targeted colonic claudin-2 expression renders resistance to epithelial injury, induces immune suppression, and protects from colitis. *Mucosal Immunol.* **7**, 1340–1353 (2014).
91. Horowitz, A., Chanez-Paredes, S.D., Haest, X. & Turner, J.R. Paracellular permeability and tight junction regulation in gut health and disease. *Nat. Rev. Gastroenterol. Hepatol.* **20**, 417–432 (2023).
92. Ramsey, B.W. et al. A CFTR potentiator in patients with cystic fibrosis and the G551D mutation. *N. Engl. J. Med.* **365**, 1663–1672 (2011).
93. Shaughnessy, C.A., Zeitlin, P.L. & Bratcher, P.E. Elexacaftor is a CFTR potentiator and acts synergistically with ivacaftor during acute and chronic treatment. *Sci. Rep.* **11**, 19810 (2021).
94. Laselva, O. et al. Rescue of multiple class II CFTR mutations by elexacaftor+tezacaftor+ivacaftor mediated in part by the dual activities of elexacaftor as both corrector and potentiator. *Eur. Respir. J.* **57**, 2002774 (2021).
95. Veit, G., Vaccarin, C. & Lukacs, G.L. Elexacaftor co-potentiates the activity of F508del and gating mutants of CFTR. *J. Cyst. Fibros.* **20**, 895–898 (2021).
96. Ito, G. et al. Lineage-specific expression of bestrophin-2 and bestrophin-4 in human intestinal epithelial cells. *PLOS ONE* **8**, e79693 (2013).
97. Strong, T., Boehm, K. & Collins, F. Localization of cystic fibrosis transmembrane conductance regulator mRNA in the human gastrointestinal tract by in situ hybridization. *J. Clin. Investig.* **93**, 347–354 (1994).
98. Trezíse, A.E. & Buchwald, M. In vivo cell-specific expression of the cystic fibrosis transmembrane conductance regulator. *Nature* **353**, 434–437 (1991).
99. Jakab, R.L., Collaco, A.M. & Ameen, N.A. Physiological relevance of cell-specific distribution patterns of CFTR, NKCC1, NBCe1, and NHE3 along the crypt-villus axis in the intestine. *Am. J. Physiol.-Gastrointest. Liver Physiol.* **300**, G82–G98 (2011).
100. Strubberg, A.M. et al. Cftr modulates Wnt/β-catenin signaling and stem cell proliferation in murine intestine. *Cell. Mol. Gastroenterol. Hepatol.* **5**, 253–271 (2018).
101. Carroll, T.D., Newton, I.P., Chen, Y., Blow, J.J. & Näthke, I. Lgr5(+) intestinal stem cells reside in an unlicensed G(1) phase. *J. Cell Biol.* **217**, 1667–1685 (2018).
102. Connolly, K.M. & Bogdanffy, M.S. Evaluation of proliferating cell nuclear antigen (PCNA) as an endogenous marker of cell proliferation in rat liver: a dual-stain comparison with 5-bromo-2'-deoxyuridine. *J. Histochem Cytochem* **41**, 1–6 (1993).
103. Tirosh, I. et al. Dissecting the multicellular ecosystem of metastatic melanoma by single-cell RNA-seq. *Science* **352**, 189–196 (2016).
104. Jin, S., Plikus, M. V. & Nie, Q. CellChat for systematic analysis of cell-cell communication from single-cell and spatially resolved transcriptomics. *bioRxiv*, 2023.2011.2005.565674 (2023).
105. Ishikawa, K. et al. Identification of quiescent LGR5+ stem cells in the human colon. *Gastroenterology* **163**, 1391–1406. e1324 (2022).
106. Borowitz, D. CFTR, bicarbonate, and the pathophysiology of cystic fibrosis. *Pediatr. Pulmonol.* **50**, S24–s30 (2015). Suppl 40.
107. Kleme, M.L. et al. CFTR deletion confers mitochondrial dysfunction and disrupts lipid homeostasis in intestinal epithelial cells. *Nutrients* **10**, 836 (2018).
108. Gustafsson, J.K. et al. Bicarbonate and functional CFTR channel are required for proper mucin secretion and link cystic fibrosis with its mucus phenotype. *J. Exp. Med.* **209**, 1263–1272 (2012).
109. Hill, D.B. et al. Pathological mucus and impaired mucus clearance in cystic fibrosis patients result from increased concentration, not altered pH. *Eur. Respiratory J.* **52**, 1801297 (2018).
110. Heijerman, H.G. et al. Efficacy and safety of the elexacaftor plus tezacaftor plus ivacaftor combination regimen in people with cystic fibrosis homozygous for the F508del mutation: a double-blind, randomised, phase 3 trial. *Lancet* **394**, 1940–1948 (2019).
111. Middleton, P.G. et al. Elexacaftor–tezacaftor–ivacaftor for cystic fibrosis with a single Phe508del allele. *N. Engl. J. Med.* **381**, 1809–1819 (2019).
112. Mornet, E. et al. Genetic differences between cystic fibrosis with and without meconium ileus. *Lancet* **331**, 376–378 (1988).
113. Byun, J. et al. Risk factors of meconium-related ileus in very low birth weight infants: patients-control study. *Sci. Rep.* **10**, (2020). 4674.
114. Kubota, A. et al. Meconium-related ileus in extremely low-birthweight neonates: etiological considerations from histology and radiology. *Pediatr. Int* **53**, 887–891 (2011).
115. Paradiso, V.F., Briganti, V., Oriolo, L., Coletta, R. & Calisti, A. Meconium obstruction in absence of cystic fibrosis in low birth weight infants: an emerging challenge from increasing survival. *Ital. J. Pediatr.* **37**, 55 (2011).

116. Szentpetery, S. et al. A case report of CFTR modulator administration via carrier mother to treat meconium ileus in a F508del homozygous fetus. *J. Cyst. Fibros.* **21**, 721–724 (2022).
117. Gómez-Montes, E. et al. Prenatal Cystic Fibrosis Transmembrane Conductance Regulator Modulator Therapy: A Promising Way to Change the Impact of Cystic Fibrosis. *Fetal Diagn. Ther.* **50**, 136–142 (2023).
118. Sun, X. et al. In utero and postnatal VX-770 administration rescues multiorgan disease in a ferret model of cystic fibrosis. *Sci. Transl. Med.* **11**, eaau7531 (2019).
119. Ooi, C.Y. et al. Impact of CFTR modulation with Ivacaftor on Gut Microbiota and Intestinal Inflammation. *Sci. Rep.* **8**, 17834 (2018).
120. Sung, S.I. et al. Increased risk of meconium-related ileus in extremely premature infants exposed to antenatal magnesium sulfate. *Neonatology* **119**, 68–76 (2022).
121. Liu, J., Walker, N.M., Cook, M.T., Ootani, A. & Clarke, L.L. Functional Cftr in crypt epithelium of organotypic enteroid cultures from murine small intestine. *Am. J. Physiol.-Cell Physiol.* **302**, C1492–C1503 (2012).
122. Gallagher, A.M. & Gottlieb, R.A. Proliferation, not apoptosis, alters epithelial cell migration in small intestine of CFTR null mice. *Am. J. Physiol.-Gastrointest. Liver Physiol.* **281**, G681–G687 (2001).
123. Liu, K. et al. Defective CFTR promotes intestinal proliferation via inhibition of the hedgehog pathway during cystic fibrosis. *Cancer Lett.* **446**, 15–24 (2019).
124. Farrell, P.M., Mischler, E.H., Engle, M.J., D Brown, J. & Lau, S.-M. Fatty acid abnormalities in cystic fibrosis. *Pediatr. Res.* **19**, 104–109 (1985).
125. Bhura-Bandali, F.N., Suh, M., Man, S.P. & Clandinin, M.T. The ΔF508 mutation in the cystic fibrosis transmembrane conductance regulator alters control of essential fatty acid utilization in epithelial cells. *J. Nutr.* **130**, 2870–2875 (2000).
126. Fondacaro, J.D., Heubi, J.E. & Kellogg, F.W. Intestinal bile acid malabsorption in cystic fibrosis: a primary mucosal cell defect. *Pediatr. Res.* **16**, 494–498 (1982).
127. Sims-Lucas, S., Goetzman, E.S. & Kleyman, T.R. Cystic fibrosis–related metabolic defects: crosstalk between ion channels and organs. *J. Clin. Investig.* **134**, e182329 (2024).
128. Mariotti Zani, E. et al. Nutritional care in children with cystic fibrosis. *Nutrients* **15**, 479 (2023).
129. Montgomery, R.K., Mulberg, A.E. & Grand, R.J. Development of the human gastrointestinal tract: twenty years of progress. *Gastroenterology* **116**, 702–731 (1999).
130. Turner, C.A., Clinton, S.M., Thompson, R.C., Watson, S.J. & Akil, H. Fibroblast growth factor-2 (FGF2) augmentation early in life alters hippocampal development and rescues the anxiety phenotype in vulnerable animals. *Proc. Natl. Acad. Sci.* **108**, 8021–8025 (2011).
131. Dettmer, R. et al. FGF2 Inhibits Early Pancreatic Lineage Specification during Differentiation of Human Embryonic Stem Cells. *Cells* **9**, 1927 (2020).
132. El Agha, E., Kosanovic, D., Schermuly, R.T. & Bellusci, S. Role of fibroblast growth factors in organ regeneration and repair. *Semin. Cell Dev. Biol.* **53**, 76–84 (2016).
133. Bikfalvi, A., Klein, S., Pintucci, G. & Rifkin, D.B. Biological roles of fibroblast growth factor-2*. *Endocr. Rev.* **18**, 26–45 (1997).
134. Houchen, C.W., George, R.J., Sturmoski, M.A. & Cohn, S.M. FGF-2 enhances intestinal stem cell survival and its expression is induced after radiation injury. *Am. J. Physiol.* **276**, G249–G258 (1999).
135. Song, X. et al. Growth factor FGF2 cooperates with interleukin-17 to repair intestinal epithelial damage. *Immunity* **43**, 488–501 (2015).
136. Xu, X. et al. Transforming growth factor-β in stem cells and tissue homeostasis. *Bone Res.* **6**, 2 (2018).
137. Koyama, S.Y. & Podolsky, D.K. Differential expression of transforming growth factors alpha and beta in rat intestinal epithelial cells. *J. Clin. Investig.* **83**, 1768–1773 (1989).
138. Chen, L. et al. TGFB1 induces fetal reprogramming and enhances intestinal regeneration. *Cell Stem Cell* **30**, 1520–1537.e1528 (2023).
139. Dignass, A.U. & Podolsky, D.K. Cytokine modulation of intestinal epithelial cell restitution: Central role of transforming growth factor β. *Gastroenterology* **105**, 1323–1332 (1993).
140. Cammareri, P. et al. TGFβ pathway limits dedifferentiation following WNT and MAPK pathway activation to suppress intestinal tumourigenesis. *Cell Death Differ.* **24**, 1681–1693 (2017).
141. Kurokowa, M., Lynch, K. & Podolsky, D.K. Effects of growth factors on an intestinal epithelial cell line: transforming growth factor β inhibits proliferation and stimulates differentiation. *Biochem. Biophys. Res. Commun.* **142**, 775–782 (1987).
142. Berková, L. et al. Terminal differentiation of villus tip enterocytes is governed by distinct Tgfβ superfamily members. *EMBO Rep.* **24**, (2023). e56454.
143. Barnard, J.A., Beauchamp, R.D., Coffey, R.J. & Moses, H.L. Regulation of intestinal epithelial cell growth by transforming growth factor type beta. *Proc. Natl Acad. Sci.* **86**, 1578–1582 (1989).
144. Barnard, J.A., Warwick, G.J. & Gold, L.I. Localization of transforming growth factor beta isoforms in the normal murine small intestine and colon. *Gastroenterology* **105**, 67–73 (1993).
145. Xiao, K. et al. TGF-β1 protects intestinal integrity and influences Smads and MAPK signal pathways in IPEC-J2 after TNF-α challenge. *Innate Immun.* **23**, 276–284 (2017).
146. Flanagan, D.J. et al. Epithelial TGFβ engages growth-factor signalling to circumvent apoptosis and drive intestinal tumourigenesis with aggressive features. *Nat. Commun.* **13**, (2022). 7551.
147. Stoeckius, M. et al. Cell Hashing with barcoded antibodies enables multiplexing and doublet detection for single cell genomics. *Genome Biol.* **19**, (2018). 224.
148. Wolock, S.L., Lopez, R. & Klein, A.M. Scrublet: Computational identification of cell doublets in single-cell transcriptomic data. *Cell Syst.* **8**, 281–291.e289 (2019).
149. Bergen, V., Lange, M., Peidli, S., Wolf, F.A. & Theis, F.J. Generalizing RNA velocity to transient cell states through dynamical modeling. *Nat. Biotechnol.* **38**, 1408–1414 (2020).
150. Jew, B. et al. Accurate estimation of cell composition in bulk expression through robust integration of single-cell information. *Nat. Commun.* **11**, (2020). 1971.
151. Dominici, M. et al. Minimal criteria for defining multipotent mesenchymal stromal cells. The International Society for Cellular Therapy position statement. *Cytotherapy* **8**, 315–317 (2006).
152. Thery, C. et al. Minimal information for studies of extracellular vesicles 2018 (MISEV2018): a position statement of the International Society for Extracellular Vesicles and update of the MISEV2014 guidelines. *J. Extracell. Vesicles* **7**, (2018). 1535750.
153. Fujii, M., Matano, M., Nanki, K. & Sato, T. Efficient genetic engineering of human intestinal organoids using electroporation. *Nat. Protoc.* **10**, 1474–1485 (2015).
154. Sato, T. et al. Paneth cells constitute the niche for Lgr5 stem cells in intestinal crypts. *Nature* **469**, 415–418 (2011).
155. Arias-Barrau, E., Dirusso, C.C. & Black, P.N. Methods to monitor Fatty Acid transport proceeding through vectorial acylation. *Methods Mol. Biol.* **580**, 233–249 (2009).

Acknowledgements

This research was funded by the Korean Fund for Regenerative Medicine (KFRM) grant funded by the Korean government (the Ministry of Science and ICT, the Ministry of Health & Welfare) (KFRM 22A0301L1 to A.K.) and the Samsung Research Funding & Incubation Center of Samsung Electronics (Project Number SRFC-MA2301-03 to A.K.). This research was also supported by the Korea Health Technology R&D Project through the Korea Health Industry Development Institute (KHIDI), funded by the Ministry of Health & Welfare, Republic of Korea (HR22C1363 to Y.S.C.), and by a grant

from the Future Medicine 2030 Project from Samsung Medical Center (SMO1240021 to S.I.S.).We thank Dr. Dong Kyung Sung for providing material support during the initial stage of the project and Prof. Jihwan Park (GIST) for valuable discussion. The graphical abstract is created in BioRender. Kim, J. (2025) https://BioRender.com/e54d113.

Author contributions

A.K. conceived the study hypothesis, supervised the project, and wrote the manuscript. S.I.S. and Y.S.C. provided material support and participated in project discussions. J.K. conducted bioinformatic analysis and co-wrote the manuscript. H.J.P. performed most of the experiments, data analysis, and co-wrote the manuscript. N.Y.P. provided technical support. S.I.H. and Y.E.K. also contributed material support. All authors reviewed the manuscript and figures.

Competing interests

The authors declare no competing interests.

Inclusion and ethics

This research was conducted in collaboration with local researchers who contributed to study design, data collection, analysis, and authorship. Ethical approval was obtained from the relevant local review board, and all research followed international ethical standards.

Additional information

Supplementary information The online version contains supplementary material available at https://doi.org/10.1038/s42003-025-07944-w.

Correspondence and requests for materials should be addressed to Se In Sung, Yun Sil Chang or Ara Koh.

Peer review information *Communications Biology* thanks Sarah Andres, Dazhi Jin, and the other, anonymous, reviewer for their contribution to the peer review of this work. Primary Handling Editors: Kuangyu Yen and Rosie Bunton-Stasyshyn.